Geochemistry, Geophysics, Geosystems

RESEARCH ARTICLE
10.1029/2022GC010662

Paleoproterozoic Plate Tectonics Recorded in the Northern Margin Orogen, North China Craton

Chen Wu[1], Guosheng Wang[2], Zhiguang Zhou[2], Peter J. Haproff[3], Andrew V. Zuza[4], and Wenyou Liu[2]

[1]State Key Laboratory of Tibetan Plateau Earth System, Environment and Resources, Institute of Tibetan Plateau Research, Chinese Academy of Sciences, Beijing, China, [2]School of Earth Sciences and Resources, China University of Geosciences, Beijing, China, [3]Department of Earth and Ocean Sciences, University of North Carolina Wilmington, Wilmington, NC, USA, [4]Nevada Bureau of Mines and Geology, University of Nevada, Reno, NV, USA

Key Points:

- Northern margin of the North China craton experienced two periods of orogenesis in the Neoarchean and Paleoproterozoic, respectively
- Northern Margin orogen of the North China craton terminated by at least ca. 1.78 Ga
- Ca. 1.77–1.73 Ga mafic dykes and ca. 1.75 Ga mylonitic shear zone are associated with a regional mantle plume event

Supporting Information:

Supporting Information may be found in the online version of this article.

Correspondence to:

C. Wu,
wuchen@itpcas.ac.cn;
wuchenlovegeology@gmail.com

Citation:

Wu, C., Wang, G., Zhou, Z., Haproff, P. J., Zuza, A. V., & Liu, W. (2022). Paleoproterozoic plate tectonics recorded in the Northern Margin orogen, North China craton. *Geochemistry, Geophysics, Geosystems*, *23*, e2022GC010662. https://doi.org/10.1029/2022GC010662

Received 10 AUG 2022
Accepted 25 OCT 2022

Author Contributions:

Conceptualization: Chen Wu, Guosheng Wang, Zhiguang Zhou
Funding acquisition: Chen Wu, Guosheng Wang, Zhiguang Zhou
Investigation: Chen Wu, Guosheng Wang, Zhiguang Zhou
Methodology: Chen Wu
Project Administration: Chen Wu
Visualization: Chen Wu, Zhiguang Zhou, Peter J. Haproff, Andrew V. Zuza, Wenyou Liu
Writing – original draft: Chen Wu
Writing – review & editing: Chen Wu, Guosheng Wang, Zhiguang Zhou, Peter J. Haproff, Andrew V. Zuza, Wenyou Liu

Abstract

The occurrence of plate tectonic processes on Earth during the Paleoproterozoic is supported by ca. 2.2–1.8 Ga subduction-collision orogens associated with the assembly of the Columbia-Nuna supercontinent. Subsequent supercontinent breakup is evidence by global ca. 1.8–1.6 Ga large igneous provinces. The North China craton is notable for containing Paleoproterozoic orogens along its margins, herein named the Northern Margin orogen, yet the nature and timing of orogenic and extensional processes of these orogens and their role in the supercontinent cycle remain unclear. In this contribution, we present new field observations, U-Pb zircon and baddeleyite geochronology dates, and major/trace-element and isotope geochemical analyses from the northern margin of the North China craton that detail its Paleoproterozoic tectonic and magmatic history. Specifically, we record the occurrence of ca. 2.2–2.0 Ga magmatic arc rocks, ca. 1.9–1.88 Ga tectonic mélange and mylonitic shear zones, and folded lower Paleoproterozoic strata. These rocks were affected by ca. 1.9–1.8 Ga granulite-facies metamorphism and ca. 1.87–1.78 Ga post-collisional, extension-related magmatism along the cratonal northern margin. We interpret that the generation and emplacement of these rocks, and the coupled metamorphic and magmatic processes, were related to oceanic subduction and subsequent continent-continent collision during the Paleoproterozoic. The occurrence of ca. 1.77–1.73 Ga mafic dykes and ca. 1.75 Ga mylonitic shear zones along the northern margin of the North China craton may have been related to a regional mantle plume event. Our results are consistent with modern style plate tectonics, including oceanic subduction-related plate convergence and continent-continent collision, operating in the Paleoproterozoic.

Plain Language Summary

Earth likely went through an early magma ocean stage, which rapidly solidified and evolved though about 4.5 billion years to the modern plate-tectonic lithosphere. Whether plate-tectonics operate in early Earth's history, is one of the hotly debated questions in Earth Sciences. The North China craton of central Asia is a natural laboratory for investigating early Earth tectonic processes including subduction-collision and large-scale horizontal crustal motions. Paleoproterozoic subduction and continent-continent collisional between the North China craton and outboard craton were associated with the assembly of the oldest-known Columbia-Nuna supercontinent. The configuration of cratons forming the supercontinent remains debated, which is partially due to an inadequate understanding of the Paleoproterozoic rocks that form the margins of the cratons and their tectonic histories. Our observations and analyses indicate the development of Paleoproterozoic Northern Margin orogen, the collisions are not just narrow belts in time and space, but rather broad, long-lived orogenic cycles that exist well within the intraplate continental interior.

1. Introduction

Modern plate tectonics on Earth is characterized by a kinematically linked global network of internally-rigid plates that rotate about Euler poles and are recycled via subduction and sea-floor spreading (e.g., Dewey, 1969; Harrison, 2020; Korenaga, 2018; A. Yin, 2012; A. Yin et al., 2020). The occurrence of modern-style plate tectonics during the Paleoproterozoic is evidenced by extensive ca. 2.0–1.8-Ga orogens (e.g., T. M. Kusky et al., 2016; B. Wan et al., 2015; Wu et al., 2018; A. Yin et al., 2020; Zhao et al., 2002). Furthermore, the Central Orogenic Belt of the North China craton has been interpreted to reflect the operation of modern-style plate tectonics, at least at a local scale, by ca. 2.7 Ga (e.g., Zhong et al., 2021, 2022). For the Central Orogenic Belt, Ning et al. (2022) reported the oldest exposed eclogite-facies oceanic crust and Huang et al. (2020) documented the

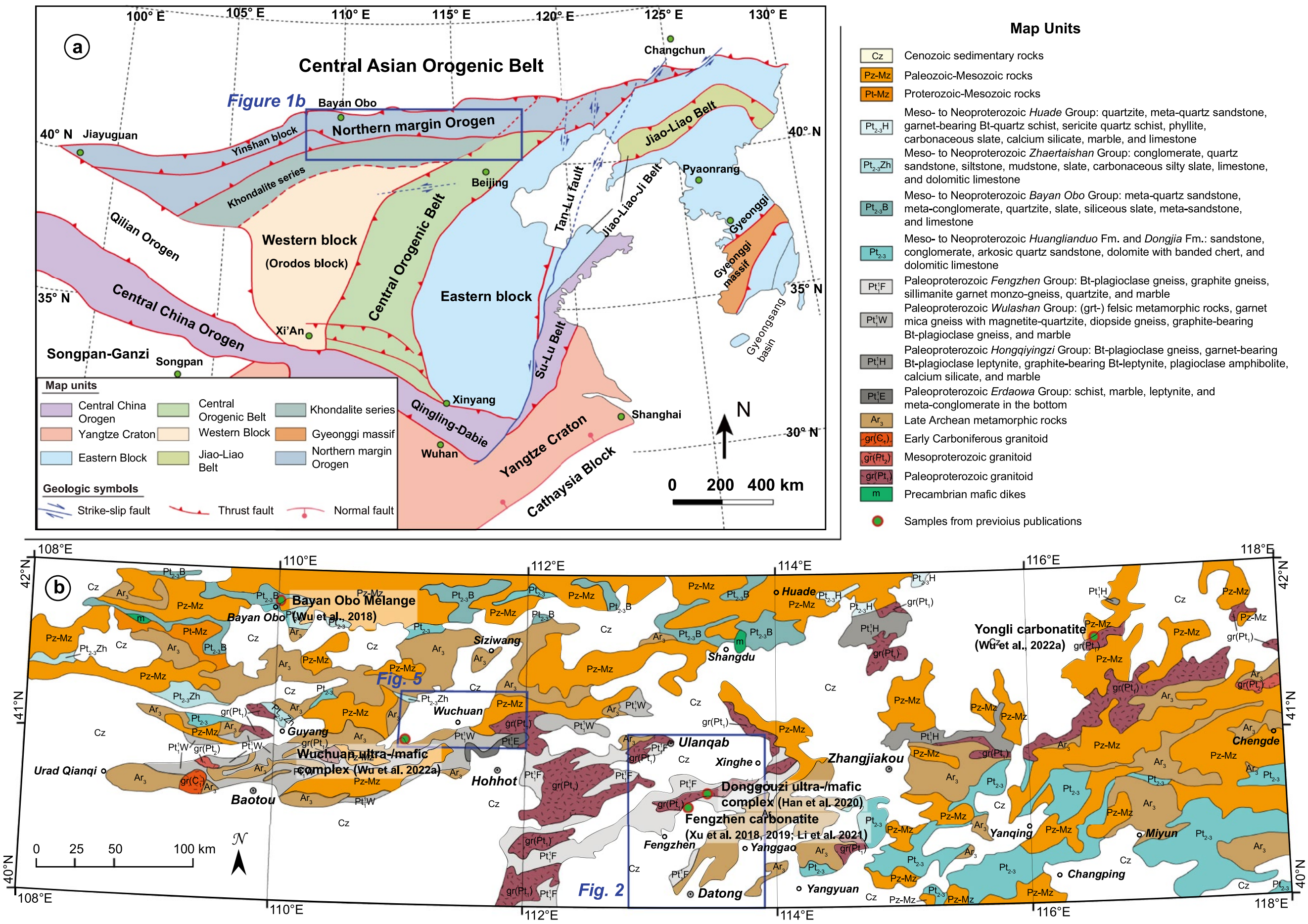

Figure 1. (a) Simplified tectonic map of the North China craton and surrounding orogenic belts, modified from Wu et al. (2018). The North China craton is divided into the Eastern and Western blocks, Central Orogenic belt, and Northern Margin orogen. (b) Simplified geological map of the northern margin of the North China craton, based on our field observations and modified from Wu, Wang, et al. (2022). The locations of detailed geological maps are shown.

occurrence of an Archean paired metamorphic belt, a fundamental characteristic of asymmetric convergent plate boundaries, indicating westward-directed subduction beneath an intra-oceanic arc along a ∼1,600-km-long belt of accretionary mélange (e.g., T. M. Kusky et al., 2016; T. Kusky et al., 2020; J. P. Wang et al., 2017, 2019; Wu, Wang, et al., 2022; Zhong et al., 2021, 2022). Alternative to interpretations of modern-style plate tectonic events, researchers have proposed that vertical plume-related tectonics involving crustal delamination and volcanic resurfacing are evidenced in the Archean–Paleoproterozoic rock record. For example, Peng et al. (2022) proposed that large igneous provinces across portions of the extinct Columbia-Nuna supercontinent reflect the occurrence of a ca. 1.8 Ga pulsating plume that was responsible for ancient plate motion.

The North China craton together with the Siberian, Baltica, Laurentian, North Australian, and Indian cratons likely formed the core of the Proterozoic Columbia-Nuna supercontinent (e.g., Meert, 2012; Rogers & Santosh, 2002; Zhao et al., 2002). The configuration of cratons forming the supercontinent remains debated, which is partially due to an inadequate understanding of the Paleoproterozoic rocks that form the margins of the cratons and their tectonic histories (Figure 1a). This problem is exemplified by the disagreement regarding the Paleoproterozoic tectonic history of the North China cratonal margins. One proposed end-member model for the tectonic development of the Paleoproterozoic North China orogen includes the formation of the southwest-trending Trans-North China orogen during the collision between the Eastern and Western blocks (e.g., Faure et al., 2007; Kröner et al., 2005, 2006; Trap et al., 2009, 2012; S. H. Zhang et al., 2007; Zhao & Cawood, 2012; Zhao et al., 2005). In this model, the Western block comprises both the Yinshan block of the northern North China margin and the Ordos block that collided with the Khondalite series at ca. 1.92 Ga. A second end-member model involves the tectonic development of the Paleoproterozoic east-trending North Margin orogen from the collision between the North China craton and outboard cratons of the Columbi-Nuna supercontinent (e.g., Han et al., 2020; T. M. Kusky & Li, 2003; T. M. Kusky et al., 2016; B. Wan et al., 2015; Wu et al., 2018; Wu, Wang et al., 2022). In this model, the ca. 1.9 Ga North Margin Orogen consists of both the Yinshan block and northern Khondalite series.

Peng et al. (2008, 2010) proposed that the northern North China margin experienced mantle upwelling and extension, followed by continent-continent collision based on the occurrence of ca. 1.80–1.78 Ga bimodal volcanic rocks (Zhao et al., 2001, 2004) and ca. 1.78–1.65 Ga rift-related magmatism and the emplacement of mafic dykes. Researchers identified an east- to northeast-trending suite of anorthosites, mangerites, charnockites, and alkali-feldspar granitoids along the northern margin of the North China craton, possibly reflecting a continent-continent collision event that terminated by 1.75 Ga (e.g., Peng et al., 2014; Rämö et al., 1995; S. H. Zhang et al., 2007). Qu et al. (2012) alternatively interpreted that this collisional event terminated at ca. 1.81 Ga based on the occurrence of hyalophane-rich pegmatite veins in high-pressure granulite bodies.

In this contribution, we integrated new and existing field observations, zircon and baddeleyite U-Pb geochronology, and whole-rock major oxide, trace element, and Sr-Nd-Pb-Hf isotope geochemistry for the northern and central portions of the North China craton. By compiling these data, we document the Paleoproterozoic tectonic evolution of the North China craton that involved Andean-type subduction and continent-continent collision along its northern margin (Figure 1b). Furthermore, detrital zircon U-Pb ages, zircon Hf and whole-rock Sr-Nd-Pb-Hf isotope statistical analyses results show that the northern margin of the North China craton experienced orogenesis in both the Neoarchean and Paleoproterozoic, which correspond to the Neoarchean Central Orogenic Belt and Northern Margin orogen, respectively.

2. Geological Setting

The North China craton is bounded by the early Paleozoic Qilian orogen to the southwest, the late Paleozoic Central Asian Orogenic System to the north, and the Mesozoic Qinling-Dabie Shan orogen to the south (Figure 1a) (e.g., Zuza & Yin, 2017). The craton consists of Archean–Paleoproterozoic metamorphic basement rocks and unmetamorphosed to weakly metamorphosed Meso- and Neoproterozoic cover successions (e.g., T. M. Kusky et al., 2016; Zhai & Santosh, 2011; Zhao et al., 2005; Zhao & Zhai, 2013). The North China craton is traditionally divided into the Archean Eastern and Western blocks that are separated by the ∼1,600-km-long, northeast-trending Neoarchean Central Orogenic Belt (e.g., T. M. Kusky & Li, 2003; T. M. Kusky et al., 2007; J. P. Wang et al., 2017, 2019; Wu et al., 2018; Wu, Li et al., 2022; Wu, Wang et al., 2022) (Figure 1a). The Central Orogenic Belt is also referred to as the Paleoproterozoic Trans-North China Orogen in the tectonic model of Zhao et al. (2001, 2005), Trap et al. (2012), and subsequent papers. It has been proposed that the Eastern Block comprises the Langrim and Lonngang blocks, which are sutured along the Paleoproterozoic Jiao-Liao-Ji orogen (e.g., Tam et al., 2011; Zhao et al., 2005). The Jiao-Liao-Ji orogen consists of ca. 3.8–2.6 Ga tonalite–trondhjemite–granodiorite gneisses (TTGs) and greenstone belts overlain by ca. 2.6–2.5 Ga metasedimentary cover rocks. However, T. M. Kusky et al. (2016) suggested that the Jiao-Liao Ji tectonic unit is a possible deformed retroarc basin and these blocks are poorly defined, much older accreted arcs. Zhao et al. (2005) suggested that the Western Block consists of the Ordos and Yinshan blocks that are sutured along the Paleoproterozoic "Khondalite belt" orogen. However, some researchers proposed that the northern margin of the North China craton is formed by the Paleoproterozoic Northern Margin orogen (e.g., B. Wan et al., 2015; Wu et al., 2018, Wu, Wang et al., 2022), also known as the Inner Mongolia-Northern Hebei orogen of T. M. Kusky et al. (2016). The Paleoproterozoic Northern Margin orogen includes the ca. 1.90–1.88 Ga Bayan Obo mélange, the Yinshan Block, and the northern "Khondalite series" (e.g., T. M. Kusky et al., 2016; Wu et al., 2018). The western continuation of the Northern Margin orogen is the Alxa block. In this context, we regard the Yinshan Block as a ribbon-shaped microcontinent comprising a Paleoproterozoic arc sequence developed upon the TTGs and metasedimentary rocks that was incorporated into the Northern Margin orogen. Furthermore, some researchers interpreted that the Archean North China craton formed via the amalgamation of at least six microcontinents along Neoarchean greenstone belts (e.g., Zhai, 2011, 2014; Zhai et al., 2021; Zhai & Santosh, 2011).

Several researchers have recorded the widespread occurrence of Paleoproterozoic (ca. 1.95–1.80 Ma) high-grade metamorphic rocks (e.g., garnet amphibolites and granulites) in the central and northern North China craton (e.g., Guo et al., 2015; Lu et al., 2008; Peng et al., 2014; Zhai & Santosh, 2011; Zhao & Zhai, 2013; Zhao et al., 2005). Zhai et al. (1992, 1993) identified a Paleoproterozoic high-pressure and high-pressure granulite rocks throughout the northern North China craton that experienced clockwise isothermal decompression P-T paths that may be

10.1029/2022GC010662

related to a continent-continent collisional event (Guo et al., 2015; Zhai, 2011). The high-pressure granulites are mainly distributed in the central portion of the craton and include the Chicheng (ultra-) high-pressure granulites, whereas the (ultra-)high-temperature granulites are mainly distributed in the northern cratonal margin (e.g., Guo et al., 2015). The ca. 2.15–1.89 Ga Hengling dyke swarms in the central North China craton experienced greenschist facies to high-pressure granulite facies metamorphism at ca. 1.9–1.8 Ga, which could be related to a continent-continent collision event (e.g., Peng, 2015; Peng et al., 2014). Ca. 2.0–1.89 Ga arc granitoids, including the ca. 2.0 Ga Banyan Obo diorites, ca. 1.97–1.93 Ga Xuwujia sill swarm, ca. 1.89 Ga dykes/volcanics, and ca. 1.93–1.90 Ga charnockites and S-type granites, also record high-temperature granulite facies metamorphism at 1.95–1.90 Ga and amphibolite to granulite facies metamorphism at ca. 1.9–1.8 Ga. These metamorphic events have been interpreted to be associated with magmatic arc accretion, followed by continent-continent collision (e.g., T. M. Kusky et al., 2016; Peng, 2015; Peng et al., 2014; Wu et al., 2018). Several researchers have postulated that late Paleoproterozoic–early Neoproterozoic rift zones developed in the North China craton, including the Xiong'er rift zone in the south, the Yanliao rift zone in the east, and the Zha'ertai–Bayan Obo–Huade rift zone in the northwest (e.g., H. Li et al., 2013; M. Li et al., 2013; C. H. Liu et al., 2020; Lu et al., 2002; Peng, 2015; Peng et al., 2014; S. H. Zhang et al., 2009, 2017; Zhou et al., 2018). In this study, we compiled existing field observations and examined key field relationships along the northern margin of the North China craton (Figure 1b).

3. Field Observations and Sampling

3.1. Paleoproterozoic Yanggao Granulite and Dykes

The crystalline basement of the Northern Margin orogen is formed by amphibolite- to granulite-facies supracrustal rocks of the Neoarchean Yanggao Formation (Figure 2). These supracrustal rocks mainly consist of quartzite, TTGs, granulite, amphibolite, and hornblende pyroxenite. Overlying the Yanggao Formation is the Paleoproterozoic Fengzhen Group, which consists of amphibolite- to granulite-facies, garnet-bearing gneiss, schist, quartzite, paragneiss, and marble interbedded with mafic metavolcanic rocks (Figure 2). The formation age of the Fengzhen Group is reported to be ca. 2.3–2.0 Ga (e.g., Peng et al., 2014; Y. S. Wan et al., 2009, 2015). The Neoarchean Yanggao Formation gneiss (sample 20-YG-02) is cut by the southeast-striking lamprophyre and diabase dykes (sample 20-YG-03) with chilled intrusion margins (Figure 3a). Meso- to Neoproterozoic clastic sedimentary rocks and carbonates overly the Neoarchean–Paleoproterozoic metamorphic basement rocks along an unconformity (Figure 2). A ~30-m-wide Yanggao plagioclase pyroxene granulite dyke (sample 19-YG-01[b]) intrudes a Paleoproterozoic hypersthene plagioclase granulite body (sample 19-YG-01[a]) (Figure 3b). The foliation within all the granulite units crosscut lithologic contacts and dip to the northeast (i.e., 155 strike, 20 {deg} NE) (Figure 3b). The granulite body is cut by a younger normal fault (Figure 3b). To the east, a lamprophyre dyke (sample 20-YG-04[b]) intrudes a hornblende hypersthene plagioclase granulite body (sample 20-YG-04[a]) and contains chilled intrusion margins (Figure 3c).

3.2. Paleoproterozoic Donggouzi Ultramafic-Mafic Complex

The northeast-trending Donggouzi ultramafic-mafic complex is elliptical in shape (~700 m long and ~200–300 m wide) and contains peridotite with internal blocks of amphibole pyroxenite and websterite (Han et al., 2020) (Figures 4a and 4b). The peridotite, amphibole pyroxenite, and websterite have been metamorphosed to amphibolite and granulite facies (Han et al., 2020). The Donggouzi ultramafic-mafic complex was cut by the syenite and mafic dykes with chilled intrusion margins (Figures 4c and 4d). The wall rocks of the ultramafic-mafic complex include TTG gneisses, high-pressure granulites, and metamorphosed Fengzhen Group supracrustal rocks. The Donggouzi ultramafic-mafic rocks and an alkali granite intrude Paleoproterozoic high-pressure granulites, all of which are unconformably overlain by Cenozoic basalts (Figure 4a). Han et al. (2020) determined the age of the Donggouzi ultramafic-mafic complex to be between ca. 1.849–1.845 Ga. They suggested that emplacement of the ultramafic-mafic complex occurred in a post-orogenic extensional setting, possibly associated with continent-continent collision along the northern margin of the North China craton at ca. 1.90–1.88 Ga. In this study, a diabase dyke sample (sample DGZ) was collected for U-Pb baddeleyite geochronology (Figure 4d).

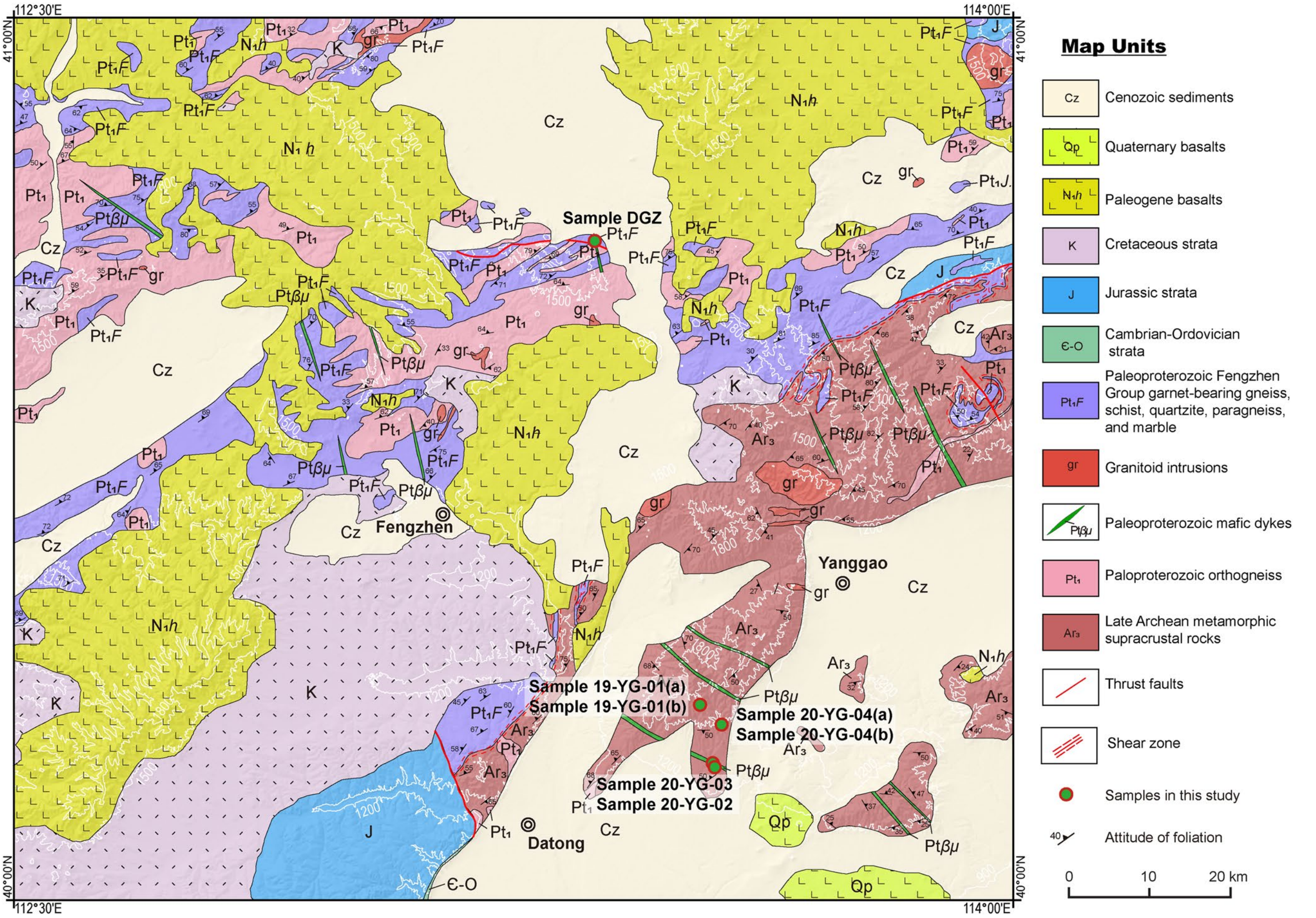

Figure 2. Simplified geological map of the Yanggao area along the northern margin of North China craton. Locations of samples collected in this study are shown.

3.3. Paleoproterozoic Wuchuan Ductile Shear Zones

The Wuchuan mylonitic shear zones occur in several lithologic units in the mapping area and contain at least two generations of shear foliation (Wu, Wang et al., 2022) (Figure 5). The older ductile shear foliation occurs in Neoarchean felsic mylonite, dolomitic marble, Neoarchean ultramafic-mafic rocks, and Paleoproterzoic gneissic granite/diorite and dykes (Figure 5). This older foliation observed in ca. 1.98 Ga diorite are crosscut by a ca. 1.87 Ga gabbro dyke. Wu, Wang, et al. (2022) interpreted that this older foliation formed via ca. 1.98–1.87 Ga left-slip ductile shear. The younger shear foliation is folded in biotite plagioclase gneiss (Figure 6a) and quartzite (sample 19-WC-06d) (Figure 6b) and occurs in marble (Figure 6c) and Paleoproterozoic granodiorite (sample 19-WC-06c). The Paleoproterozoic granodiorite is intruded by undeformed plagioclase amphibolite (sample 19-WC-06a) and diorite (sample 19-WC-06b) (Figures 6d and 6e). We used this intrusional contact to constrain the age of the ductile shear associated with the younger foliation. The presence of shear folds within the quartzite, mineral stretching lineation and rotated porphyroclast in mylonitized marble are interpreted to have formed during a regional extensional event.

3.4. Paleoproterozoic Bayan Obo Mélange and Yongli Carbonatite

The Bayan Obo mélange, one of the oldest documented sedimentary mélanges on Earth, contains a structurally complex tectonic mixture of metapelites, metapsammites, and mica-quartz schist matrix. These rocks are mixed with exotic blocks of ultramafic and metagabbroic rocks and metabasalts that locally include possible relict pillow structures, plagiogranite, amphibolite, carbonatite, alkaline granulite, and TT gneisses. Zircon $^{207}Pb/^{206}Pb$ ages of various blocks in the Bayan Obo mélange demonstrate that the formation and associated deformation of age of

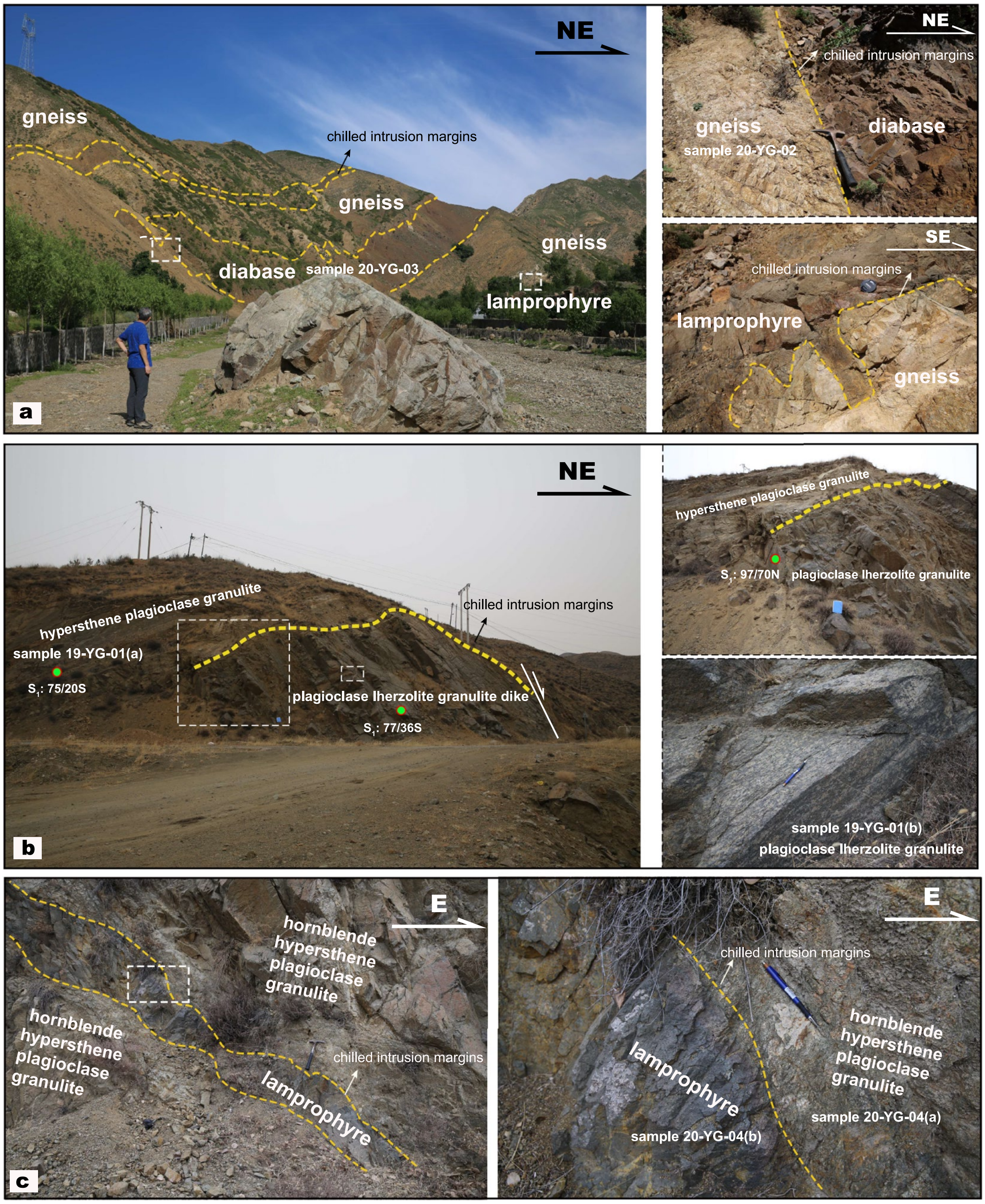

Figure 3. Field photographs showing key geological relationships of the Yanggao area. (a) Yanggao diabase and lamprophyre intruding gneiss; (b) plagioclase lherzolite granulite dyke intruding a hypersthene plagioclase granulite body; and (c) lamprophyre intruding hornblende hypersthene plagioclase granulite with a well-defined chilled intrusion margin.

the mélange is ca. 1.9 Ga (Wu et al., 2018). Rocks of the Bayan Obo mélange were deposited near the subduction trench, based on the mixing of upper and lower plate volcanic rocks and textural relationships within the mélange (Wu et al., 2018). The ~300–400-m-wide and ~1-km-long, northwest-southeast-elongated Yongli carbonatite pluton intrudes Hongqiyingzi Group metamorphic rocks and is itself intruded by syenogranite. Subvertical, northwest-striking fluorite veins within the carbonatite pluton are ~10–50 cm wide. Numerous subangular and subelliptical xenoliths of amphibolite and pyroxene biotite plagioclase gneiss occur within the carbonatite and range in width from >10 m to ~5–10 cm. The long axes of the xenoliths are oriented northwest-southeast, mirroring the shape of the larger host carbonatite pluton. Wu, Wang, et al. (2022) reported a protolith age of

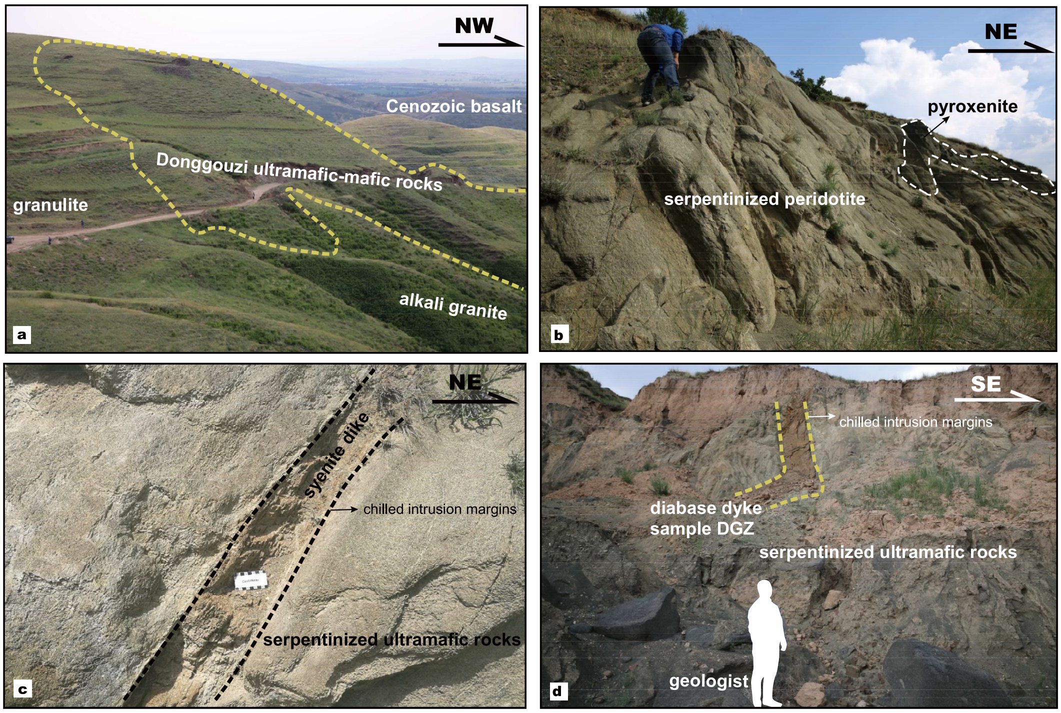

Figure 4. Field photographs showing key geological relationships of the Donggouzi area. (a) Contact between the Donggouzi mafic-ultramafic complex and wall rocks; (b) pyroxenite blocks occurring as lenses within peridotite; and (c) a syenite dyke; and (d) diabase dyke intruding serpentinized ultramafic rocks with a well-defined chilled intrusion margin.

ca. 1.862 Ga for the Yongli carbonatite pluton. Geochemistry results of Yongli carbonatite show ocean island basalt-like characteristics, which may be indicative of within-plate magmatism (Wu, Wang, et al., 2022).

3.5. Petrologic Observations

Petrographic observations were made on representative samples of key outcrops to constrain the setting of their petrogenesis. Plagioclase amphibolite sample 19-WC-06(a) contains plagioclase (vol. ∼55%), hornblende (vol. ∼35%), quartz (vol. ∼5%), and biotite (vol. ∼5%) (Figure 7a). Diorite sample 19-WC-06(b) contains plagioclase (vol. ∼70%), hornblende (vol. ∼20%), quartz (vol. ∼5%), and biotite (vol. ∼10%) (Figure 7b). Mylonitized granodiorite sample 19-WC-06(c) contains plagioclase (vol. ∼60%), potassium feldspar (vol. ∼15%), quartz (vol. ∼20%), and biotite (vol. ∼5%) (Figure 7c). Diabase sample DGZ contains plagioclase (vol. ∼60%), pyroxene (vol. ∼40%), and minor biotite (Figure 7d). Hypersthene plagioclase granulite sample 19-YG-01(a) contains plagioclase (vol. ∼65%), quartz (vol. ∼15%), hypersthene (vol. ∼15%), garnet (vol. ∼5%), and minor biotite (Figure 7e). Plagioclase lherzolite granulite sample 19-YG-01(b) contains plagioclase (vol. ∼45%), hornblende (vol. ∼5%), diopside and hypersthene (vol. ∼50%), and minor biotite (Figure 7f). Hornblende hypersthene plagioclase granulite sample 20-YG-04(a) contains plagioclase (vol. ∼40%), hornblende (vol. ∼40%), pyroxene (vol. ∼15%), biotite (vol. ∼5%), and minor quartz (Figure 7g). Diabase sample 20-YG-03 contains plagioclase (vol. ∼70%), pyroxene (vol. ∼20%), and olivine (vol. ∼10%) (Figure 7h).

4. Analytical Methods and Results

4.1. U-Pb Zircon Geochronology

Zircon grains used for U-Pb geochronology were separated from eight samples using traditional methods involving crushing, sieving, and magnetic and density separations. Individual zircon grains were picked under a binocular microscope and mounted in epoxy with standard zircon grains. Cathodoluminescence images of zircon grains were collected using a JXA-880 electron microscope with operating conditions of 20 kV and 20 nA at the Institute of Mineral Resources, Chinese Academy of Geological Sciences, Beijing. Zircon grains were analyzed

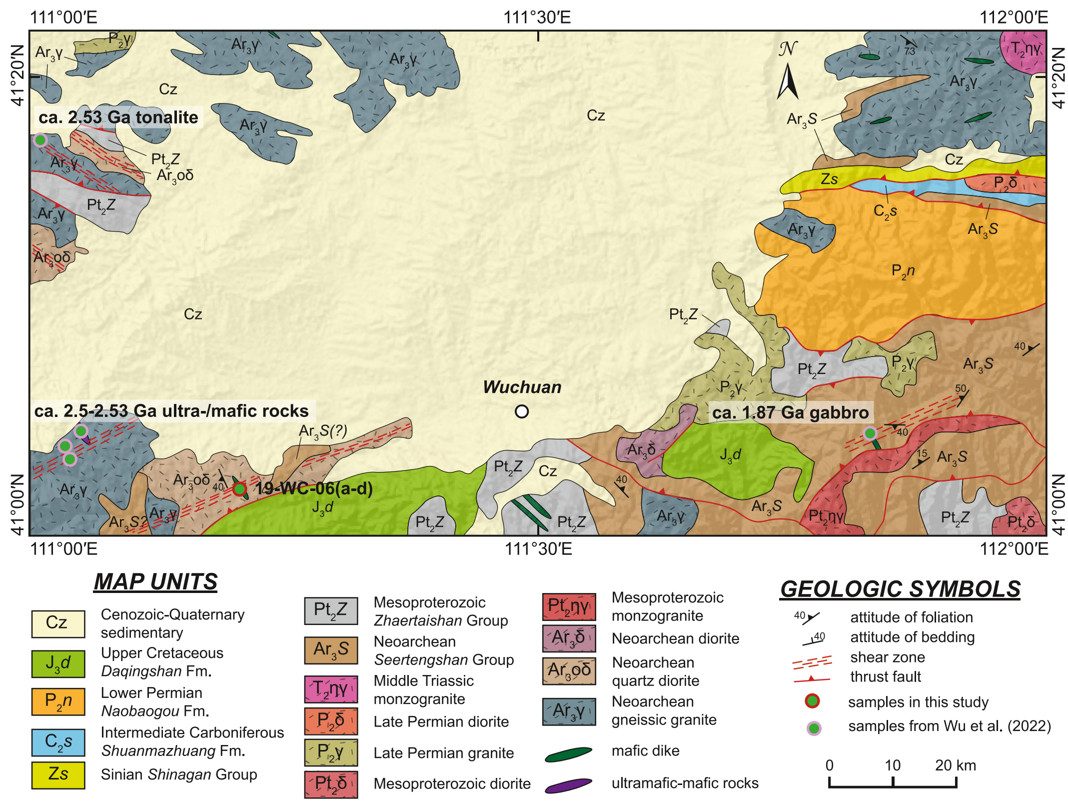

Figure 5. Simplified geological map of the Wuchuan area, located along the northern margin of North China craton. Locations of samples collected in this study are shown.

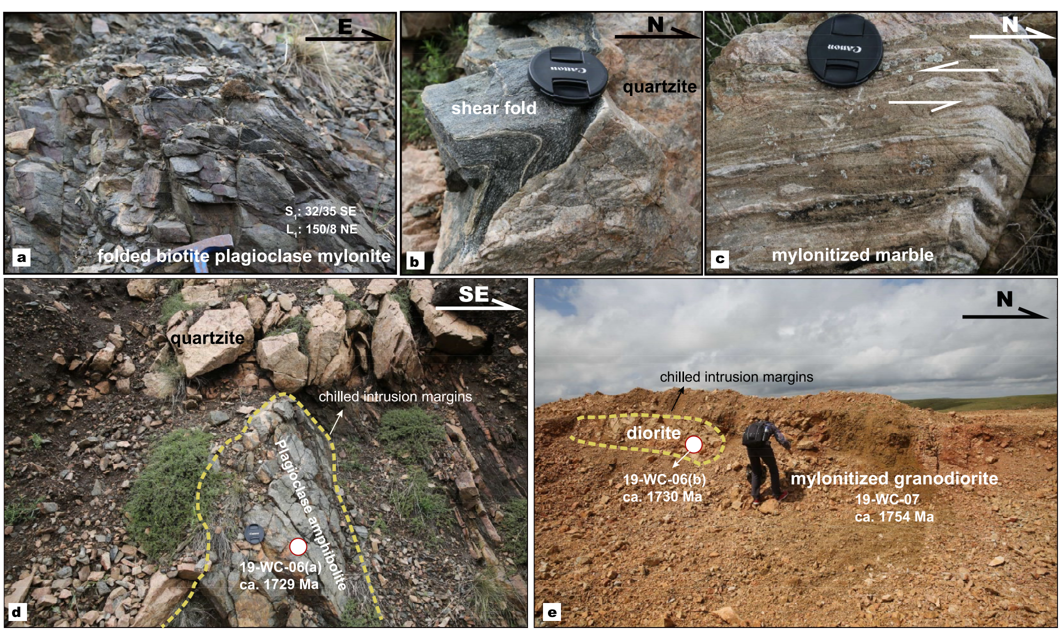

Figure 6. Field photographs showing key geological relationships of the Wuchuan area, including foliation associated with ductile shear occurring in (a) folded biotite plagioclase mylonite; (b) folded quartzite; and (c) marble. Undeformed plagioclase amphibolite and diorite intruding (d) quartzite and (e) mylonitized granodiorite, respectively.

10.1029/2022GC010662

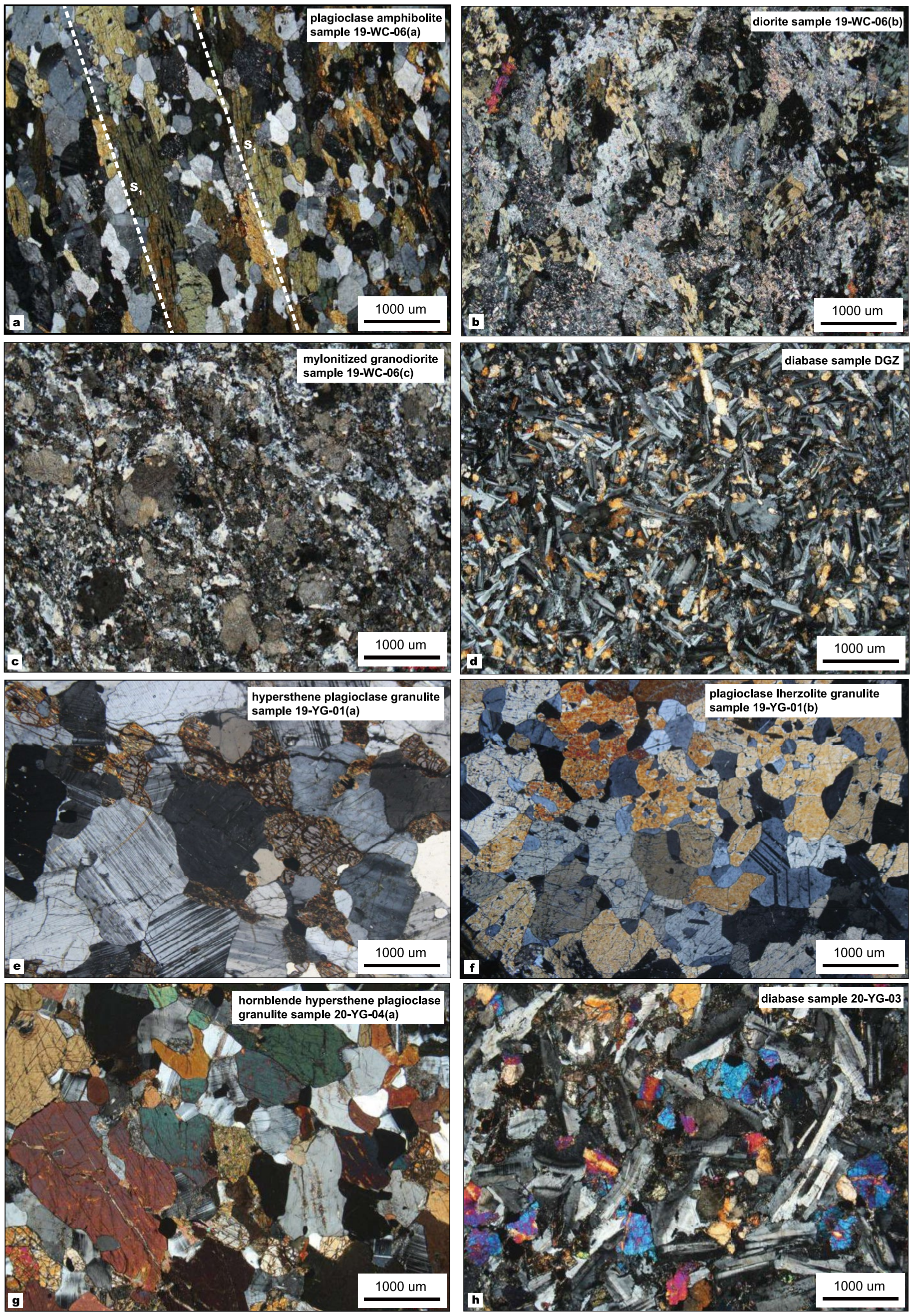

Figure 7. Representative photomicrographs of samples collected in this study.

via inductively coupled plasma mass spectrometry (ICP-MS) using an Agilent 7500a instrument coupled with a New Wave Research UP193FX Excimer Laser Ablation System at the Key Laboratory of Continental Collision and Plateau Uplift, Institute of Tibetan Plateau Research, Chinese Academy of Sciences, Beijing. Common Pb corrections were performed assuming an initial Pb composition from Stacey and Kramers (1975). The primary standard used was GJ1 (Jackson et al., 2004). Secondary standards included 91,500 ($^{238}U/^{206}Pb$ age of 1,065 Ma; Wiedenbeck et al., 1995) and Plesovice ($^{238}U/^{206}Pb$ age of 337 Ma; Sláma et al., 2008). Reported U-Pb ages are $^{206}Pb^*/^{207}Pb^*$ ages for grains older than 1,000 Ma and $^{206}Pb^*/^{238}U^*$ ages for grains younger than 1,000 Ma. Crystallization ages are interpreted from analyses with <10% discordance. Concordia diagrams and weighted mean U-Pb ages were processed using Isoplot v.3 (Ludwig, 2003). Age data and concordia plots are reported with 2σ error. Uncertainties of weighted mean ages are presented at the 95% confidence level (Figure 8). Sample

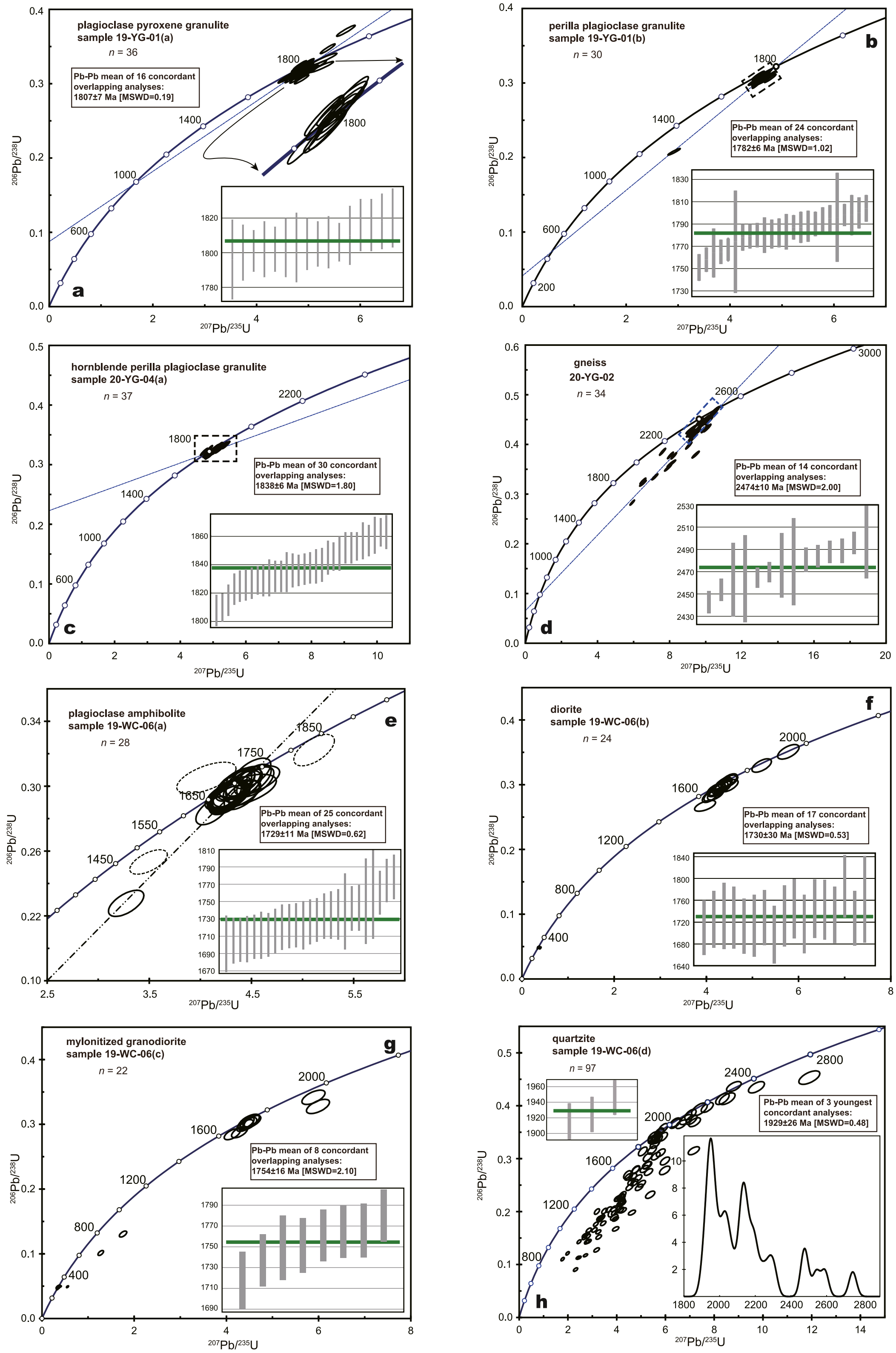

Figure 8. Zircon U-Pb concordia plots of eight samples. MSWD is mean square of weighted deviates. See Table 1 for sample locations and Table S1 in Supporting Information S1 for details of analyses.

10.1029/2022GC010662

Table 1
Summary of Sample Locations and Geochronology Results From This Study

Sample	Description	Latitude (°N)	Longitude (°E)	Elevation (m)	Zircon U-Pb age (Ma)	MSWD	*n*
19-YG-01(a)	Hypersthene plagioclase granulite	40°23′12.1″	113°40′14.2″	1,189	1,807 ± 7	0.19	16 out of 36
19-YG-01(b)	Plagioclase lherzolite granulite	40°23′12.1″	113°40′14.2″	1,189	1,782 ± 6	1.02	24 out of 30
20-YG-04(a)	Hornblende hypersthene plagioclase granulite	40°17′43″	113°32′4″	1,572	1,838 ± 6	1.8	30 out of 37
20-YG-02	Gneiss	40°14′13.5″	113°35′20.6″	1,364	2,474 ± 10	2	14 out of 34
19-WC-06(a)	Plagioclase amphibolite	41°2′21.8″	111°16′9.6″	1,636	1,729 ± 11	0.62	25 out od 28
19-WC-06(b)	Diorite	41°2′21.8″	111°16′9.6″	1,636	1,730 ± 30	0.53	17 out of 24
19-WC-06(c)	Mylonitized granodiorite	41°2′21.8″	111°16′9.6″	1,636	1,754 ± 16	2.1	8 out of 22
Sample	Description	Latitude (°N)	Longitude (°E)	Elevation (m)	Detrital zircon MDA (Ma)	MSWD	*n*
19-WC-06(d)	Quartzite	41°2′21.8″	111°16′9.6″	1,636	1,929 ± 26	0.48	3 out of 97
Sample	Description	Latitude (°N)	Longitude (°E)	Elevation (m)	Baddeleyite U-Pb age (Ma)	MSWD	*n*
19-YG-01(a)	Hypersthene plagioclase granulite	40°23′12.1″	113°40′14.2″	1,189	1,802 ± 16	2	19 out of 20
20-YG-04(b)	Lamprophyre	40°17′43″	113°32′4″	1,572	1,782 ± 6	0.75	19 out of 19
20-YG-03	Diabase	40°14′13.5″	113°35′20.6″	1,364	1,769 ± 9	0.83	17 out of 20
DGZ	Diabase	40°40′39.25″	113°30′10.09″	1,316	1,778 ± 10	1.8	19 out of 19

Note. MSWD, mean square weighted deviation; MDA, maximum depositional age.

locations and U-Pb zircon geochronology results are shown in Table 1. Details of geochronology analyses are shown in Table S1 of Supporting Information S1.

Three granulite samples were collected for zircon U-Pb geochronology. Thirty-six zircon grains analyzed from hypersthene plagioclase granulite sample 19-YG-01(a) yield Pb-Pb ages between 1,753 and 1,931 Ma (Figure 8a). The weighted mean of 16 concordant analyses is 1,807 ± 7 Ma (MSWD = 0.19) (Figure 8a). Thirty zircon grains analyzed from plagioclase lherzolite granulite sample 19-YG-01(b) yield Pb-Pb ages between 1,737 and 1,850 Ma (Figure 8b). The weighted mean of 24 concordant analyses is 1,782 ± 6 Ma (MSWD = 1.02) (Figure 8b). Thirty-seven zircon grains analyzed from hornblende hypersthene plagioclase granulite sample 20-YG-04(a) yield Pb-Pb ages between 1,743 and 1,920 Ma (Figure 8c). The weighted mean of 16 concordant analyses is 1,838 ± 6 Ma (MSWD = 1.8) (Figure 8c). Thirty-four zircon grains analyzed from gneiss sample 20-YG-02 yield Pb-Pb ages between 2,268 and 2,547 Ma (Figure 8d). The weighted mean of 14 concordant analyses is 2,474 ± 10 Ma (MSWD = 2) (Figure 8d). Twenty-eight zircon grains analyzed from plagioclase amphibolite sample 19-WC-06(a) yield Pb-Pb ages between 1,556 and 1,881 Ma (Figure 8e). The weighted mean of 25 concordant analyses is 1,729 ± 11 Ma (MSWD = 0.62) (Figure 8e). Twenty-four zircon grains were analyzed from diorite sample 19-WC-06(b) yield a U-Pb age of ca. 304 Ma and a Pb-Pb age of ca. 1,949 Ma. The weighted mean of 17 concordant analyses is 1,730 ± 30 Ma (MSWD = 0.53) (Figure 8f). Twenty-two zircon grains were analyzed from mylonitized granodiorite sample 19-WC-06(c) yield a U-Pb age of ca. 289 Ma and a Pb-Pb age of ca. 2,132 Ma (Figure 8g). The weighted mean of eight concordant analyses is 1,754 ± 16 Ma (MSWD = 2.1) (Figure 8g). One hundred zircon grains analyzed from the quartzite sample 19-WC-06(d) yield Pb-Pb ages between 1,916 and 2,747 Ma. The weighted mean of the three youngest concordant zircon grains is 1,929 ± 26 Ma (MSWD = 0.48) (Figure 8h), which we interpret is the maximum depositional age of the quartzite sample. This quartzite sample has two major zircon populations with two peaks at ca. 1.95 and ca. 2.14 Ga. A minor age population occurs at ca. 2.48 Ga (Figure 8h).

4.2. U-Pb Baddeleyite Geochronology

U-Pb baddeleyite analyses were conducted via laser ablation ICP-MS at the Beijing Geo-Analysis Laboratory. Detailed operating conditions for laser ablation using the ICP-MS instrument and data reduction follow those of Xie et al. (2008). Laser ablation was performed using a NWR193 system with a 193-nm excimer laser source. An Agilent 7500 ICP-MS instrument was used to acquire ion signal intensities. He was applied as a carrier gas.

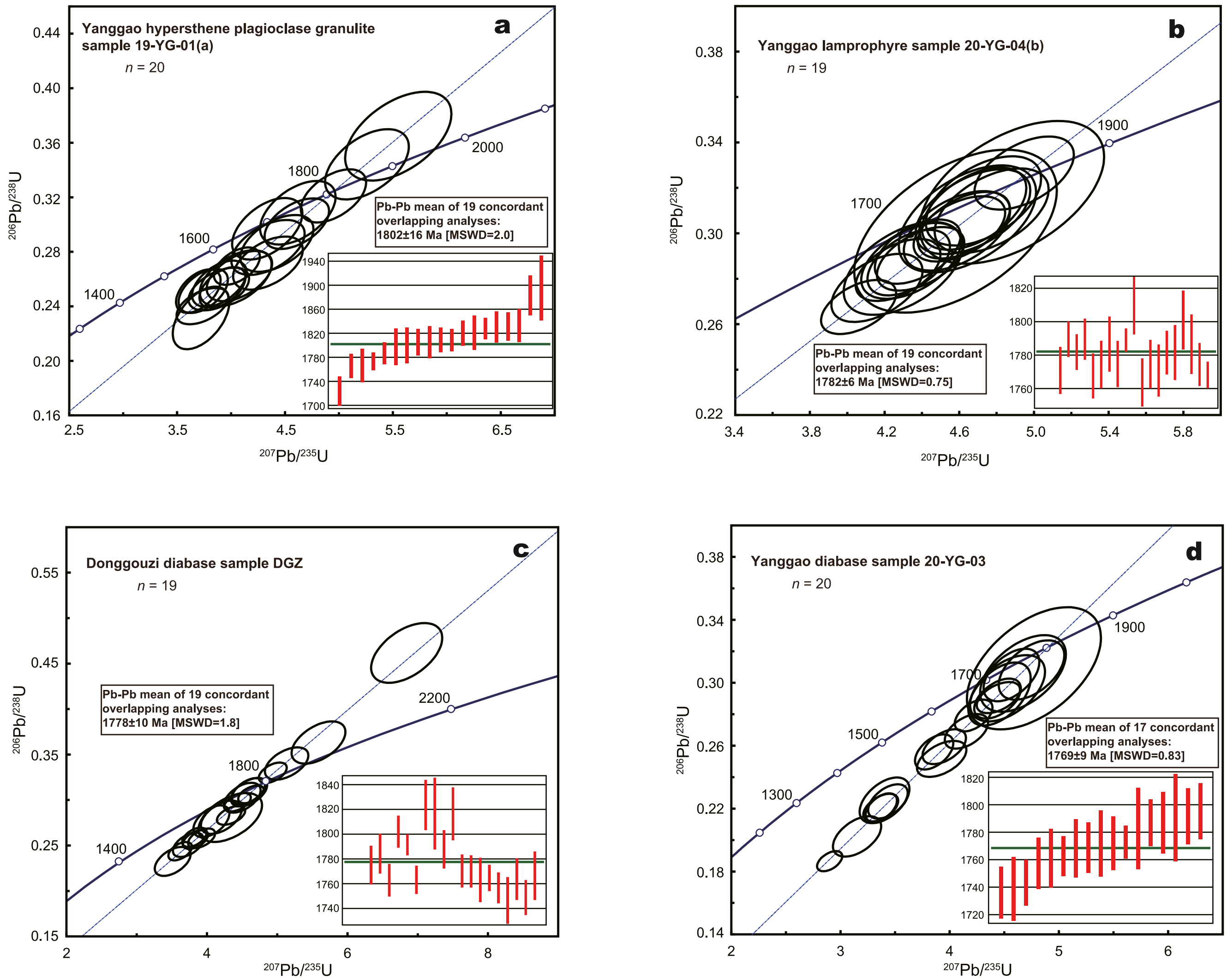

Figure 9. Baddeleyite U-Pb concordia plots of four samples. MSWD is mean square of weighted deviates. See Table 1 for sample locations and Table S2 in Supporting Information S1 for details of analyses.

Ar was used as the make-up gas and mixed with He via a T-connector before entering the ICP-MS instrument. Each analysis incorporated a background acquisition of approximately 15 seconds (gas blank) followed by 45 s of data acquisition from the sample. Off-line raw data selection and integration of background, analytical signals, time-drift correction, and quantitative calibration for U-Pb dating were performed using ICPMSDataCal. All measurements were performed using the Phalaborwa baddeleyite with a $^{207}Pb/^{206}Pb$ age of 2,059.8 ± 0.8 Ma (Heaman & LeCheminant, 1993) as the external standard and monitoring sample. The geochronologic data were processed using Isoplot v.3 (Ludwig, 2003). Sample locations and U-Pb baddeleyite geochronology results are shown in Table 1. Details of geochronologic analyses are shown in Table S2 of Supporting Information S1.

Twenty baddeleyite grains analyzed from hypersthene plagioclase granulite sample 19-YG-01(a) yield Pb-Pb ages between 1,724 and 1,896 Ma (Figure 9a). The weighted mean of 19 concordant analyses is 1,802 ± 16 Ma (MSWD = 2.0) (Figure 9a). Nineteen baddeleyite grains analyzed from lamprophyre sample 20-YG-04(b) yield Pb-Pb ages between 1,765 and 1,813 Ma (Figure 9b). The weighted mean of 19 concordant analyses is 1,782 ± 6 Ma (MSWD = 0.75) (Figure 9b). Nineteen baddeleyite grains analyzed from Donggouzi diabase sample DGZ yield Pb-Pb ages between 1,748 and 1,828 Ma (Figure 9c). The weighted mean of 19 concordant analyses is 1,778 ± 10 Ma (MSWD = 1.8) (Figure 9c). Twenty baddeleyite grains analyzed from Yanggao diabase dyke sample 20-YG-03 yield Pb-Pb ages between 1,736 and 1,795 Ma (Figure 9d). The weighted mean of 17 concordant analyses is 1,769 ± 9 Ma (MSWD = 0.83) (Figure 9d).

4.3. Whole-Rock Geochemistry and Sr-Nd-Pb-Hf Isotope

Three granulite and seven diabase samples were analyzed for their whole-rock major oxide, trace elements, and Sr-Nd-Pb-Hf isotope compositions at the Wuhan Sample Solution Analytical Technology Co., Ltd. in Hubei, China to determine the setting of their petrogenesis. Prior to analysis, weathered surfaces were removed from whole-rock samples. Samples were then crushed and ground into powder (>200 mesh) using a ball mill. Major element compositions were determined via X-ray fluorescence spectrometry with analytical accuracy better than 2%. Trace element compositions were measured via ICP-MS with analytical accuracy better than 5%. Sr-Nd-Pb-Hf isotopes were measured using a Neptune Plus multi-collector ICP-MS with spectral analysis accuracy better than 0.002%. Prior to isotope analysis, sample dissolution was performed using acid digestion (HF + HCLO4 + HNO3). Background isotope measurements were conducted within the error range. Aliquots of NIST SRM 987, JNDI-1, and JMC international standard solutions were regularly used for evaluating the reproducibility and accuracy of the instrument. Analytical results of standard sample BCR-2 (basalt) include $^{143}Nd/^{144}Nd$ = 0.512641 ± 11 (2 S.D.), $^{87}Sr/^{86}Sr$ = 0.705012 ± 22 (2 S.D.), $^{208}Pb/^{204}Pb$ = 38.736 ± 17, $^{207}Pb/^{204}Pb$ = 15.628 ± 3, $^{206}Pb/^{204}Pb$ = 18.756 ± 10 (2 S.D.), and $^{176}Hf/^{177}Hf$ = 0.282864 ± 14 (2 S.D.) (W. Zhang & Hu, 2020). Data reduction for analyses of Sr isotope ratios was conducted using Iso-Compass software (W. Zhang et al., 2020). Whole-rock geochemical and Sr-Nd-Pb-Hf isotopic results are presented in Tables 2 and 3, respectively.

Three Paleoproterozoic (ca. 1,802 Ma) Yanggao granulite samples (19-YG-01[a]) have SiO_2 of 46.30–47.30 wt% and high MgO of 5.86%–8.36% and Ni of 64.1–84.6 ppm (Table 2). Chondrite-normalized rare earth element (REE) patterns of the three granulite samples are characterized by slight light rare earth element (LREE) enrichment (LaN/YbN = 1.4–2.8) and flat heavy rare-earth element (HREE) slopes with a slight negative anomaly Eu anomaly (Eu/Eu* = 0.83–0.96) (Figure 10a). In primitive mantle-normalized spider diagrams, the three granulite samples are enriched in high-field strength elements (HFSEs; e.g., Nb, Ta) and depleted in large-ion lithophile elements (LILES; e.g., Th, U) (Figure 10b). Compared to the granulite samples, three ca. 1,782 Ma Yanggao lamprophyre samples (20-YG-04[b]) have higher SiO_2 of 52.93–54.24 wt.% and lower MgO of 4.43–4.63 wt.% and Ni of 39.9–41.1 ppm (Table 2). Chondrite-normalized REE patterns of Paleoproterozoic lamprophyre samples are characterized by significant LREE enrichment and HREE depletion (La_N/Yb_N = 28.7–30.5) with a slightly negative Eu anomaly (Eu/Eu* = 0.87–0.93) (Figure 10a). In primitive mantle-normalized spider diagrams, the three lamprophyre samples are enriched in large-ion lithophile elements (LILES; e.g., Th, U, Ba, K) and depleted in high-field strength elements (HFSEs; e.g., Nb, Ta, Ti) (Figure 10b).

Three ca. 1,769-Ma Yanggao diabase samples (20-YG-03) have SiO_2 of 43.38–45.69 wt%, high MgO of 8.96%–10.25%, and Ni of 35.9–46.7 ppm (Table 2). Chondrite-normalized REE patterns of these samples are characterized by strong LREE enrichment and HREE depletion (LaN/YbN = 46.3–54.9) with no obvious Eu anomaly (Eu/Eu* = 0.88–0.90) (Figure 10a). In primitive mantle-normalized spider diagrams, the three samples are enriched in large-ion lithophile elements (LILES; e.g., Th, U, K) and depleted in high-field strength elements (HFSEs; e.g., Nb, Ta and Ti) (Figure 10b). Three ca. 1,778 Ma Donggouzi diabase samples (DGZ) have SiO_2 of 47.35–47.67 wt%, MgO of 4.57%–4.65%, and Ni of 39.1–41.4 ppm (Table 2). Chondrite-normalized REE patterns of these samples are characterized by moderate LREE enrichment and HREE depletion (La_N/Yb_N = 10.4) with a slight negative Eu anomaly (Eu/Eu* = 0.89–0.91) (Figure 10a). In primitive mantle-normalized spider diagrams, the three samples are depleted in large-ion lithophile elements (LILES; e.g., Th, U, K) and enriched in high-field strength elements (HFSEs; e.g., Nb, Ta and Ti) (Figure 10b).

Three ca. 1,802 Ma Yanggao granulite samples (19-YG-01[a]) have consistent initial $^{87}Sr/^{86}Sr$ ratios of 0.703707–0.704703 and varied $\varepsilon Nd(t)$ values of −0.9 to +1.4 and $\varepsilon Hf(t)$ of −3.75 to +10.89 (Table 3). A single sample yields $^{206}Pb/^{204}Pb(t)$ and $^{207}Pb/204Pb(t)$ ratios of 15.3096 and 15.0501, respectively (Table 3). Four ca. 1,769 Ma Yanggao diabase samples (20-YG-03) have consistent initial $^{87}Sr/^{86}Sr$ ratios of 0.704514–0.704982 and negative $\varepsilon Nd(t)$ values of −7.4 to −21.3 and $\varepsilon Hf(t)$ values of −14.78 to −15.49 (Table 3). These four samples yield $^{206}Pb/^{204}Pb(t)$ and $^{207}Pb/^{204}Pb(t)$ ratios of 17.42147–17.48499 and 15.44904–15.45377, respectively (Table 3). Four ca. 1,778 Ma Donggouzi diabase samples (DGZ) have consistent lower initial $^{87}Sr/^{86}Sr$ ratios of 0.702440–0.702552, negative $\varepsilon Nd(t)$ values of −7.4 to −12.0 and $\varepsilon Hf(t)$ values of −5.76 to −5.84 (Table 3). The four samples yield $^{206}Pb/^{204}Pb(t)$ and $^{207}Pb/^{204}Pb(t)$ ratios of 16.77401–17.27311 and 15.3549–15.44719, respectively (Table 3).

Table 2
Whole-Rock Geochemistry Data of the Yanggao Granulite, Lamprophyre, Diabase, and Donggouzi Diabase Samples From This Study

	Granulite sample 19-YG-01(a)			Lamprophyre sample 20-YG-04(b)			Diabase sample 20-YG-03			Diabase sample DGZ		
SiO_2	47.3	46.3	46.37	53.29	52.93	54.24	43.38	45.69	44.15	47.63	47.35	47.67
Al_2O_3	14.03	12.23	12.58	15.68	15.67	15.8	4.67	4.34	3.93	15.34	15.28	15.3
CaO	13.72	10.7	9.98	4.95	4.81	4.59	17.59	18.38	19.88	6.38	6.39	6.28
$Fe_2O_3^T$	12.53	19.81	20.01	8.15	8.03	8.01	16.69	14.91	13.31	15.6	15.41	14.97
FeO	9.45	13.33	13.69	3.99	3.99	3.84	9.23	7.36	7.29	10.81	10.17	9.81
K_2O	0.2	0.38	0.35	3.26	3.27	2.98	2.46	1.91	1.75	2.03	2.03	2.04
MgO	8.36	5.88	5.86	4.49	4.43	4.63	9.31	8.96	10.25	4.65	4.57	4.65
MnO	0.21	0.25	0.24	0.11	0.11	0.09	0.25	0.27	0.22	0.17	0.17	0.16
Na_2O	1.61	1.73	1.76	4.15	4.15	4.77	0.91	1.2	1.05	3.48	3.45	3.43
P_2O_5	0.09	0.29	0.3	0.74	0.73	0.72	2.16	1.99	3.02	0.82	0.81	0.81
TiO_2	0.88	2.07	2.05	1.49	1.5	1.48	1.37	1.1	1.18	3.23	3.2	3.14
H_2O+	0.68	0.62	0.54	2.72	2.78	2.28	0.68	0.66	0.88	1.94	1.92	2.06
Li	12.7	12.6	11.9	26.8	26.3	20.8	9.18	8.93	9.09	13.2	12.8	14.2
Be	0.25	0.72	0.96	2.13	1.6	1.98	2.71	3.19	2.65	2.1	1.75	1.83
Mn	1,629	1,976	1,897	838	796	680	1,946	2,072	1,765	1,310	1,278	1,290
Co	52.9	60.1	59.2	23.4	22.4	23.3	50.3	46.6	46.7	42.7	42	44
Ni	84.6	65.9	64.1	41.1	39.9	40.6	35.9	46.7	45.4	39.9	39.1	41.4
Cu	124	108	129	19.7	19.9	19.5	109	110	256	35.5	38.9	32
Zn	79.5	137	135	127	121	125	104	90.1	82.9	155	154	156
Ga	13.2	17.4	19.8	19.1	18.9	19.5	10.8	8.51	8.66	23.5	22.7	23.4
Rb	1.3	2.83	2.35	58.2	57	47.1	55.9	36.3	53.3	31.9	30.1	32.4
Sr	153	152	120	999	960	952	2,635	2,561	3,164	703	687	719
Mo	0.09	0.48	0.38	0.76	0.7	0.9	0.4	0.48	0.54	1.7	1.72	1.66
Cd	0.05	0.08	0.1	0.08	0.08	0.05	0.08	0.08	0.18	0.07	0.07	0.05
In	0.06	0.14	0.11	0.06	0.06	0.06	0.12	0.16	0.12	0.09	0.09	0.08
Cs	0.14	0.14	0.18	0.47	0.41	0.37	6.81	11.1	8.16	0.83	0.71	0.74
Ba	25.6	162	159	1,578	1,568	1,462	2,965	2,639	1,835	1,016	1,005	1,042
Tl	0.05	0.05	0.05	0.46	0.43	0.36	0.35	0.33	0.32	0.06	0.05	0.06
Pb	1.31	0.69	0.81	10.9	10.3	11.2	12.9	9.26	11.1	9.02	6.6	6.24
Bi	0.05	0.05	0.05	0.05	0.05	0.05	0.15	0.08	0.27	0.05	0.05	0.05
Th	0.13	0.09	0.12	4.29	4.07	4.35	12.1	9.83	8.69	2.83	2.7	2.89
U	0.05	0.05	0.05	1.06	1.01	1.09	1.8	1.8	1.27	0.71	0.7	0.69
Nb	3.54	6.72	6.49	20	19.4	20.4	9.31	7.73	6.44	31.5	31.1	32.1
Ta	0.29	0.49	0.44	1.13	1.17	1.14	0.31	0.46	0.26	1.89	1.88	1.95
Zr	36.2	95.6	90.7	245	235	249	180	222	124	308	301	313
Hf	1.19	2.96	2.8	5.75	5.49	5.89	5.48	6.7	4.03	7.42	7.42	7.69
Ti	4,830	13,095	13,009	8,012	7,758	8,002	7,153	5,707	6,377	20,619	19,934	20,943
W	0.1	0.08	0.15	0.45	0.36	0.33	0.28	0.38	0.31	0.3	0.3	0.25
As	0.57	0.53	0.73	1.74	2.31	1.59	0.93	0.62	1.09	2.9	0.71	1.04
V	265	497	498	148	142	148	354	301	273	208	201	210
La	3.77	13.6	13.4	55.6	54.8	56.9	120	118	150	44.3	42.1	44.8
Ce	9.67	32.9	31.9	110	107	112	274	270	334	91.7	87.9	92.9
Pr	1.47	4.77	4.52	13.6	13	13.8	31.6	30.9	38.7	12	11.4	12.2

Table 2
Continued

	Granulite sample 19-YG-01(a)			Lamprophyre sample 20-YG-04(b)			Diabase sample 20-YG-03			Diabase sample DGZ		
Nd	7.64	23.3	21.7	56.1	53.7	56	124	123	149	53.3	51.7	56
Sm	2.15	5.77	5.29	9.09	8.74	9.21	21.9	21.6	25.3	10.5	10.2	10.9
Eu	0.76	1.72	1.65	2.48	2.29	2.36	5.71	5.54	6.68	3.03	2.98	3.1
Gd	2.75	6.91	5.94	6.65	6.33	6.85	15.9	15.8	18.7	9.65	9.38	9.99
Tb	0.48	1.14	0.94	0.79	0.73	0.79	1.64	1.63	1.98	1.33	1.27	1.34
Dy	3.13	7.18	6.14	3.86	3.81	3.89	7.24	7.06	8.5	7.22	7.13	7.36
Ho	0.65	1.48	1.22	0.65	0.63	0.65	1.07	1.06	1.26	1.3	1.27	1.34
Er	2.02	4.54	3.74	1.77	1.68	1.78	2.74	2.58	3.07	3.72	3.58	3.84
Tm	0.3	0.61	0.52	0.23	0.2	0.23	0.29	0.3	0.33	0.48	0.46	0.48
Yb	1.95	4.1	3.47	1.39	1.29	1.35	1.78	1.83	1.96	3.05	2.89	3.09
Lu	0.3	0.63	0.54	0.22	0.2	0.21	0.27	0.3	0.3	0.46	0.45	0.46
Sc	46.7	44.4	42	15.4	14.3	14.8	46.6	42.8	56.3	18.3	18	18.6
Y	18.1	40.1	34.2	18.6	17.9	18.9	28.7	27.2	34.1	35.5	34	36.6

5. Discussion

5.1. Paleoproterozoic Granulites and Dykes of the Northern North China Craton

Crystallization ages of the Yanggao granulites in the northern North China craton based on our U-Pb zircon geochronology define three groups: (a) ca. 1,838 ± 6 Ma hornblende hypersthene plagioclase granulite; (b) ca. 1,807 ± 7 Ma hypersthene plagioclase granulite; and (c) ca. 1,782 ± 6 Ma plagioclase pyroxene granulite. The U-Pb baddeleyite age of the hypersthene plagioclase granulite of ca. 1,802 ± 16 Ma is similar to its zircon crystallization age. In this section, we use the U-Pb baddeleyite age of ca. 1.802 Ga for the crystallization age of the hypersthene plagioclase granulite for the purpose of discussion, because the slight younger baddeleyite age is closer to the magmatism. Geochemistry results of the ca. 1.802 Ga Yanggao granulite samples show E-MORB characteristics, which may be indicative of petrogenesis in a back-arc extensional setting. Sr-Nd-Pb-Hf isotope compositions also support the interpretation of petrogenesis in a post-collisional, continental magmatic arc setting during the Paleoproterozoic, possibly sourced from a partially melted, subducted oceanic slab. We observed that the ca. 1.802 Ga hypersthene plagioclase granulite body was cut by the ca. 1.782 Ga plagioclase pyroxene granulite intrusion. We also observed that the ca. 1.782 Ga lamprophyre dyke intrudes the ca. 1.838 Ga hornblende hypersthene plagioclase granulite. The ca. 1.782 Ga Yanggao lamprophyre dyke show OIB geochemical characteristics, which may be indicative of petrogenesis in an intraplate magmatic setting. From these observations and results, we interpret that the ca. 1.838–1.782 Ga granulites and ca. 1.782 Ga lamprophyre dyke were generated in a post-collisional extensional setting within the Northern Margin orogen of the North China craton.

Numerous high-pressure granulites occur throughout the northern Central Orogenic belt, including granulites within the Huai'an-Xuanhua area with metamorphic ages of ca. 1.85–1.80 Ga (e.g., Guo et al., 2001; Peng et al., 2005; J. Wang et al., 2010; Zhao et al., 2008), the Chicheng area with metamorphic ages of ca. 1.90–1.91 Ga (H. Liu & Zhang, 2021; D. D. Zhang et al., 2021), and the Chengde area with metamorphic ages of ca. 1.84–1.81 Ga (H. C. Zhang et al., 2022). Clockwise P-T paths were identified in all high-pressure granulites (e.g., Guo et al., 2015; H. Liu & Zhang, 2021; D. D. Zhang et al., 2021; H. C. Zhang et al., 2022), which were interpreted to be related to continent-continent collision. The occurrence of (ultra-)high-temperature granulites along the northern margin of the North China craton was initially reported by Jin (1989). Santosh, Tsunogae, et al. (2007) and Santosh, Wilde, et al. (2007) reported the timing of the peak metamorphism to be ca. 1.92 Ga. Based on field relationships and geochronological data, researchers have interpreted that the (ultra-)high-temperature metamorphism was cogenetic with the emplacement of ca. 1.93–1.91 Ga, mantle-derived gabbro dykes possibly related to subduction of a spreading ridge (e.g., Guo et al., 2012; Peng et al., 2010). Thus, the ca. 1.78–1.90 Ga high-grade metamorphism is not confined to Central Orogenic Belt, but also occurred along the Northern Margin orogen of the North China craton (e.g., Han et al., 2020; T. M. Kusky & Li, 2003; T. M.

Table 3
Whole-Rock Sr-Nd-Pb-Hf Isotope of the Yanggao Granulite, Diabase, and Donggouzi Diabase Samples From This Study

Sample no.	Rock type	Rb (ppm)	Sr (ppm)	$^{87}Rb/^{86}Sr$	$^{87/86}Sr$	$(^{87}Sr/^{86}Sr)$ T	T (Ma)
19-YG-01(a)	Yanggao granulite	2.83	152	0.0539	0.706103	0.704703117189694	1,807
19-YG-01(a)	Yanggao granulite	2.35	120	0.0567	0.706232	0.704759548730351	1,807
19-YG-01(a)	Yanggao granulite	1.3	153	0.0246	0.704346	0.703707257095433	1,807
20-YG-03	Yanggao diabase	53.3	3,164	0.0487	0.706007	0.704767383067328	1,769
20-YG-03	Yanggao diabase	55.9	2,635	0.0614	0.706075	0.704513899569315	1,769
20-YG-03	Yanggao diabase	36.3	2,561	0.0410	0.706023	0.704979975542522	1,769
20-YG-03	Yanggao diabase	36.3	2,561	0.0410	0.706025	0.704981975338416	1,769
DGZ	Donggouzi diabase	32.4	719	0.1304	0.705868	0.702534973469671	1,778
DGZ	Donggouzi diabase	30.1	687	0.1267	0.705793	0.70255237168544	1,778
DGZ	Donggouzi diabase	31.9	703	0.1313	0.705796	0.702439745006032	1,778

Sample no.	Rock type	Sm (ppm)	Nd (ppm)	$^{147}Sm/^{144}Nd$	$^{143/144}Nd$	$(^{143/144}Nd)$ T	$\varepsilon Nd(t)$	T (Ma)
19-YG-01(a)	Yanggao granulite	5.77	23.3	0.149696204331978	0.512079	0.510299428609964	−0.027690154784654	1,807
19-YG-01(a)	Yanggao granulite	5.29	21.7	0.14735998358842	0.512008	0.510256201335496	−0.874784083325642	1,807
19-YG-01(a)	Yanggao granulite	2.15	7.64	0.170095644927658	0.512396	0.510373922388656	1.43211105682495	1,807
20-YG-03	Yanggao diabase	25.3	149	0.176116718211698	0.512022	0.509972627895915	−7.39976997991332	1,769
20-YG-03	Yanggao diabase	21.9	124	0.186316438509538	0.512023	0.509854939434876	−9.70580304624713	1,769
20-YG-03	Yanggao diabase	21.6	123	0.227115319700897	0.512022	0.509379185590718	−19.0279072387378	1,769
20-YG-03	Yanggao diabase	21.6	123	0.237315039998736	0.512024	0.509262497129678	−21.3143459196408	1,769
DGZ	Donggouzi diabase	10.9	56	0.196516158807377	0.512257	0.509958549090298	−7.4464172956501	1,778
DGZ	Donggouzi diabase	10.2	51.7	0.206715879105217	0.512261	0.509843253269845	−9.70561986377683	1,778
DGZ	Donggouzi diabase	10.5	53.3	0.216915599403057	0.512263	0.509725957449391	−12.0040121017295	1,778

Sample no.	Rock type	Lu(ppm)	Hf(ppm)	$^{176}Lu/^{177}Hf$	$^{176/177}Hf$	$(^{176/177}Hf)$T	$\varepsilon Hf(t)$	T(Ma)
19-YG-01(a)	Yanggao granulite	0.63	2.96	1.13740337878673	0.282837	0.282836961733951	2.29735798333186	1,802
19-YG-01(a)	Yanggao granulite	0.54	2.8	1.0306267350639	0.282666	0.282665965326274	−3.74978983726071	1,802
19-YG-01(a)	Yanggao granulite	0.3	1.19	1.3472244902796	0.28308	0.283079954674868	10.8906041985413	1,802
20-YG-03	Yanggao diabase	0.3	4.03	0.39781566834559	0.282354	0.28235398686125	−14.7826532990059	1,769
20-YG-03	Yanggao diabase	0.27	5.48	0.263298800928733	0.282334	0.28233399130397	−15.4897797951925	1,769
20-YG-03	Yanggao diabase	0.3	6.7	0.239283155736228	0.282339	0.28233899209714	−15.3129308430455	1,769
DGZ	Donggouzi diabase	0.46	7.69	0.319666530550089	0.282608	0.282607989388586	−5.80006188626525	1,778
DGZ	Donggouzi diabase	0.45	7.42	0.324096457567263	0.282609	0.282608989241534	−5.76470290619469	1,778
DGZ	Donggouzi diabase	0.46	7.42	0.331298601068758	0.282607	0.282606989002457	−5.83543972189182	1,778
DGZ	Donggouzi diabase	0.46	7.42	0.331298601068758	0.282609	0.282608989002457	−5.76471136095713	1,778

Sample no.	Rock type	Pb (ppm)	Th (ppm)	U (ppm)	$^{206}Pb/^{204}Pbt$	$^{207}Pb/^{204}Pbt$	$^{208}Pb/^{204}Pbt$	T (Ma)
19-YG-01(a)	Yanggao granulite	1.31	0.13	0.05	15.3096347492831	15.0501102274147	35.2329424657437	1,802
20-YG-03	Yanggao diabase	11.1	8.69	1.27	17.4221269924605	15.4510416761034	37.6044062236691	1,769
20-YG-03	Yanggao diabase	12.9	12.1	1.8	17.4214727748961	15.4490444527752	37.6289881333911	1,769
20-YG-03	Yanggao diabase	9.26	9.83	1.8	17.4799999551498	15.4524654325938	37.6582153954864	1,769
20-YG-03	Yanggao diabase	9.26	9.83	1.8	17.4849918812659	15.4537650408027	37.6544009601658	1,769
DGZ	Donggouzi diabase	6.24	2.89	0.69	16.7740079701606	15.3549046959825	36.9848822461089	1,778
DGZ	Donggouzi diabase	6.6	2.7	0.7	16.8910652834905	15.3767452532142	37.1091353061692	1,778
DGZ	Donggouzi diabase	9.02	2.83	0.71	17.2731139383589	15.4471858797625	37.443618262056	1,778

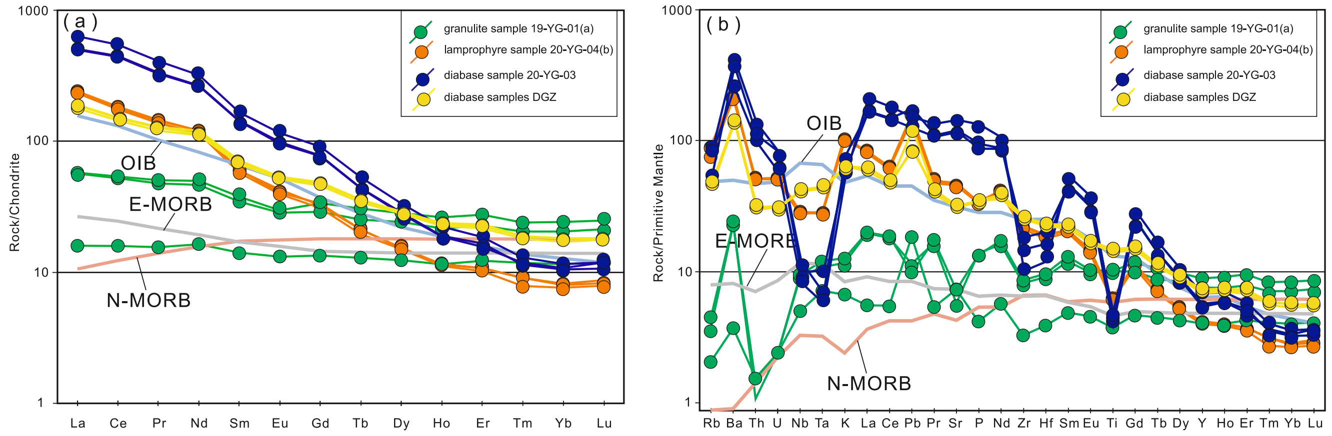

Figure 10. (a) Chondrite-normalized rare earth element and (b) primitive mantle-normalized, multi-element patterns of 12 samples. The values for normal mid-ocean ridge basalt (N-MORB), enriched mid-ocean ridge basalt (E-MORB), ocean-island basalt (OIB), and primitive mantle (PM) are from McDonough and Sun (1995).

Kusky et al., 2007, 2016; Peng et al., 2014; Wei et al., 2019; Wu et al., 2018; Wu, Wang, et al., 2022; D. Xiao et al., 2021) (Figure 11).

We observed that ca. 2.474 Ga gneiss of the Yanggao Formation was cut by a northwest-trending, ca. 1.769 Ga diabase dyke. The ca. 2.474 Ga age of the Yanggao Formation gneiss is consistent with the ca. 2.5 Ga age of metamorphic supracrustal rocks of the Yanggao Formation (Figure 2). In addition, the Donggouzi ultramafic-mafic complex intrudes the ca. 1.849 Ga Fengzhen granulite and is itself intruded by ca. 1.845 Ga syenite, ca. 1.767 Ga gabbro, and ca. 1.778 Ga diabase dykes (Han et al., 2020; this study). Major oxide, trace element, and Sr-Nd isotope geochemical compositions of ca. 1.767 Ga gabbro samples suggest that they formed in an intraplate extensional setting and experienced crustal contamination. This late Paleoproterozoic magmatism may have been related to the interaction of an upwelling mantle plume with the lithosphere (Han et al., 2020). Geochemical

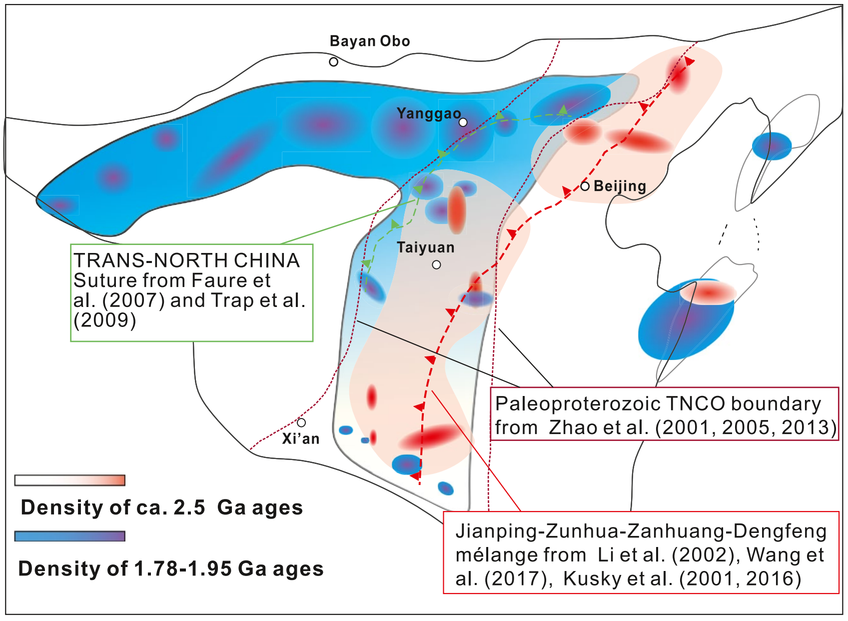

Figure 11. Simplified tectonic map of the North China Craton. The shade of different colors represents the density of distribution of ca. 2.5 Ga and 1.78–1.95 Ga ages. Note that the ca. 2.5 Ga metamorphism is consistent with the Jianpin g-Zunhua-Zanhuang-Dengfeng suture, whereas the 1.78–1.95 Ga metamorphism is widely distributed in the entire North China craton but becomes weaker from north to south, and the high-grade metamorphism is mainly developed in the northern craton. Note: TNCO, Trans-North China Orogen. Data from D. Xiao et al. (2021), Guo et al. (2015), and D. D. Zhang et al. (2021).

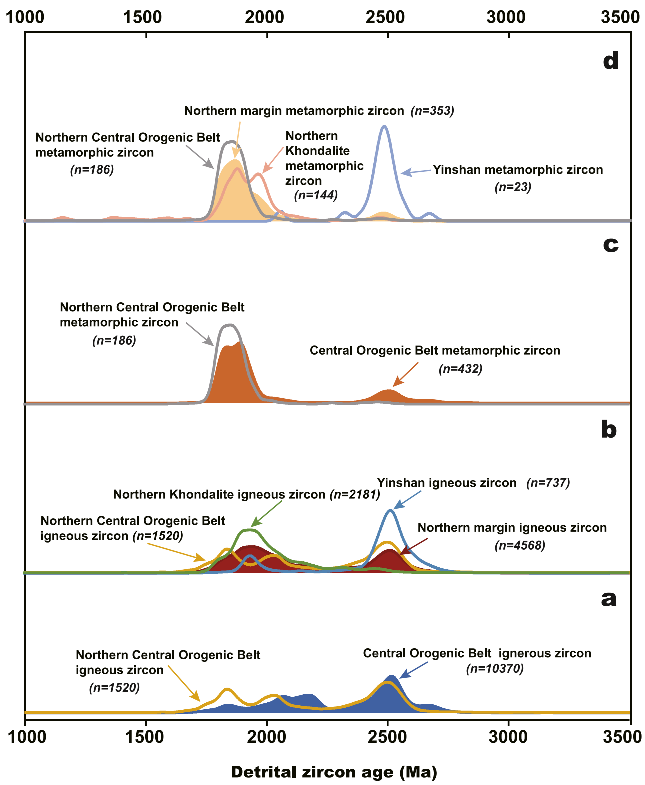

Figure 12. Normalized relative probability plots of detrital zircon U-Pb ages of samples from the Central Orogenic Belt and Northern Margin orogen.

compositions of the Yanggao and Donggouzi diabase dykes show OIB characteristics, which may be indicative of petrogenesis in an intraplate extensional setting. Sr-Nd-Pb-Hf isotope compositions of the dykes suggest an enriched mantle source, possibly derived from an upwelling mantle plume that interacted with the lithosphere. This interpretation is supported by the geochemical composition of the Yanggao diabase that shows strong fractionation, possibly related to partial melting of enriched lithospheric mantle. Major oxide, trace element, and Sr-Nd-Pb-Hf isotope geochemical compositions of the ca. 1.767–1.778 Ga Yanggao and Donggouzi diabase and gabbro dykes suggest that they were generated from a late Paleoproterozoic mantle plume within the North China craton. From these results, we interpret that magmatism and deformation related to continent-continent collision to form the Northern Margin orogen terminated by ca. 1.78 Ga.

5.2. Detrital Zircon Ages and Isotope Concentrations From the Northern North China Craton

Few Neoarchean and Paleoproterozoic magmatic and metamorphic rocks are exposed in the North China craton due to multiple phases of Phanerozoic overprinting (e.g., Zuza & Yin, 2017). To mitigate this issue, we compiled detrital zircon crystallization ages and isotope concentrations to constrain the Neoarchean–Paleoproterozoic magmatic and metamorphic history of the Northern Margin orogen. Previous studies of the North China craton have focused on the central orogen between the Eastern and Western blocks. Here, we place the Neoarchean and Paleoproterozoic orogens of the North China craton as the "Yinshan Block," "Northern Central Orogenic Belt," and northern "Khondalite series" (Figure 1a). Zircon $^{207}Pb/^{206}Pb$ ages were used and divided into two groups according to their Th/U ratios indicative of an igneous origin (Th/U ratio >0.1) or metamorphic origin (Th/U ratio <0.1). Previous researchers have established that magmatism in the Eastern Block peaked at 2.7 Ga and 3.3 Ga, whereas magmatism in the Western Block peaked at ca. 1.9 Ga (e.g., Y. S. Wan et al., 2015). Our compilation for the Central Orogenic Belt (n = 10,370) shows the occurrence three distinct Neoarchean–Paleoproterozoic igneous age populations of ca. 2.60–2.45 Ga, ca. 2.2–2.0 Ga, and ca. 1.90–1.75 Ga with four peaks at ca. 2.52 Ga, ca. 2.15 Ga, ca. 2.05 Ga, and ca. 1.83 Ga (e.g., Cai et al., 2017; Chen et al., 2015; Cui et al., 2015; Diwu et al., 2008, 2010, 2013; Du et al., 2011, 2012, 2016, 2017; Duan et al., 2014, 2018; Gao & Santosh, 2019; Geng et al., 2012; Hu et al., 2012; C. Lan et al., 2017; Z. Lan et al., 2014; H. Li et al., 2013; M. Li et al., 2013; Q. Li et al., 2011; Q. Li, Liu,Wang, Chu, et al., 2008; Q. Li, Liu, Wang, Zhang, et al., 2008; X. Y. Li et al., 2020; C. H. Liu et al., 2014; C. H. Liu, Zhao, Liu, et al., 2012; C. H. Liu, Zhao, Sun, Wu, et al., 2011; C. H. Liu, Zhao, Sun, Zhang et al., 2011; C. H. Liu, Zhao, Sun, Zhang, & Yin, 2012; C. H. Liu, Zhao, Sun, Zhang, Yin, & He, 2012; C. H. Liu, Liu, et al., 2016; C. H. Liu, Zhao, et al., 2016; J. H. Liu et al., 2020; X. Liu et al., 2020; Lyu et al., 2019; M. Z. Ma et al., 2012; X. Ma et al., 2014; X. Ma, Fan, et al., 2013; X. Ma, Guo, et al., 2013; J. Meng et al., 2018; Y. Meng et al., 2018; Peng et al., 2017; L. Ren et al., 2013; R. Ren et al., 2011; Santosh et al., 2015; Shi et al., 2018; Sun et al., 2017, 2020; Tang et al., 2016; Y. S. Wan et al., 2006, 2010, 2011, 2012, 2015; F. Wang et al., 2011; J. Wang et al., 2010; J. P. Wang et al., 2017, 2019; M. Wang et al., 2020a, 2020b; X. Wang et al., 2017; Xia et al., 2006, 2008, 2009; L. L. Xiao et al., 2019; H. F. Zhang et al., 2014, 2016, 2017, 2019; Zhu et al., 2011, 2019; P. Zuo, Li, Liu, et al., 2019; P. Zuo, Li, Zhang, et al., 2019; X. Zuo et al., 2019) (Figures 12a and 12b). In addition, our compilation shows that the northern Central Orogenic Belt (n = 1,520) exhibits three igneous age populations of ca. 2.6–2.4 Ga, ca. 2.10–1.98 Ga, and ca. 1.90–1.72 Ga with peaks at ca. 2.5 Ga, ca. 2.05 Ga, and ca. 1.83 Ga (e.g., Cai et al., 2017; Dan et al., 2012; Ding et al., 2018; C. Dong et al., 2007, 2013, X. Dong et al., 2012; Duan et al., 2018; Fan et al., 2010; Jian et al., 2005, 2012; Jiao et al., 2013; W. X. Li et al., 2022; X. P. Li et al., 2011; C. H. Liu et al., 2014; L. C. Liu et al., 2012; X. Ma et al., 2014; X. Ma, Fan, et al., 2013; X. Ma, Guo, et al., 2013; R. Ren et al., 2011; Y. S. Wan et al., 2006, 2011; C. Wang et al., 2015; D. Wang & Guo, 2017; D. Wang et al., 2015; F. Wang et al., 2011; J. Wang et al., 2010; L. Wang et al., 2015; X. Wang et al., 2017; Wu et al., 2018; Xia et al., 2006; Yang et al., 2014; C. Q. Yin et al., 2009, 2011; X. H.

Zhang et al., 2014, and this study) (Figures 11c and 11d). These three igneous age populations for the northern Central Orogenic Belt are similar to those for entire Central Orogenic Belt with the exception of the ca. 2.15 Ga peak. The northern margin of the North China craton (n = 4,568) exhibits two main zircon age populations of ca. 2.60–2.45 Ga and ca. 2.20–1.72 Ga with two respective peaks of ca. 2.5 Ga and ca. 1.95 Ga (Figures 12c and 12d). Two metamorphic episodes recorded in both the Central Orogenic Belt (n = 432) and Northern Margin orogen (n = 353) have well-defined age populations of ca. 2.58–2.43 and ca. 1.98–1.77 Ma with respective peaks of ca. 2.5 and ca. 1.85 Ga (Figures 12b and 12d). Previous studies have focused on the metamorphic ages of ca. 1.98–1.77 Ga with a peak at ca. 1.85 Ga in the Central Orogenic Belt (e.g., Zhao et al., 2005, 2012). However, metamorphism recorded at ca. 2.5 Ga should also be considered for the Central Orogenic Belt and Northern Margin orogen, which was overprinted by ca. 1.93–1.80 Ga, granulite-facies metamorphism. We interpret that this Neoarchean tectono-thermal event was associated with an arc-continent collisional event along the Zanhuang-Dongwanzi-Zunhua ophiolitic mélange to form the Central Orogenic Belt (e.g., T. M. Kusky et al., 2016; T. Kusky et al., 2021, 2022; Ning et al., 2022; J. P. Wang et al., 2017, 2019; Zhong et al., 2021).

The zircon εHf(t)-age evolution of Central Orogenic Belt suggest an overall continuous evolution from ca. 2.7–1.8 Ga (e.g., Chen et al., 2015; Cui et al., 2015; Diwu et al., 2008, 2013; Du et al., 2012, 2016, 2017; Geng et al., 2012; Hu et al., 2012, 2014; Q. Li et al., 2011; X. Y. Li et al., 2020; C. H. Liu et al., 2014; C. H. Liu, Liu, et al., 2016; C. H. Liu, Zhao, et al., 2016; C. H. Liu, Zhao, Liu, et al., 2012; C. H. Liu, Zhao, Sun, Wu, et al., 2011; C. H. Liu, Zhao, Sun, Zhang et al., 2011; C. H. Liu, Zhao, Sun, Zhang, & Yin, 2012; C. H. Liu, Zhao, Sun, Zhang, Yin, & He, 2012; J. Meng et al., 2018; Y. Meng et al., 2018; L. Ren et al., 2013; R. Ren et al., 2011; Santosh et al., 2015; Shi et al., 2018; Sun et al., 2017; Y. S. Wan et al., 2011, 2015; F. Wang et al., 2011; X. Wang et al., 2017; Xia et al., 2008, 2009; H. F. Zhang et al., 2016; Zhu et al., 2011) (Figure 13a). In contrast, the zircon εHf(t)-age evolution of Northern Margin orogen suggests two distinct episodes at ca. 2.7–2.2 Ga and ca. 2.10–1.75 Ga (e.g., Dan et al., 2012; C. Dong et al., 2007; X. He et al., 2017; W. X. Li et al., 2022; X. Ma, Fan, et al., 2013; X. Ma, Guo, et al., 2013; R. Ren et al., 2011; Y. S. Wan et al., 2011; C. Wang et al., 2015; D. Wang et al., 2015; F. Wang et al., 2011; L. Wang et al., 2015; Xia et al., 2008; Yang et al., 2014; C. Q. Yin et al., 2011; X. H. Zhang et al., 2014) (Figure 12b). These results support the interpretation that the Central Orogenic Belt developed in the Neoarchean, while the Northern Margin orogen experienced two orogenic events in the Neoarchean and Paleoproterozoic. The εHf(t) versus age plots for the Central Orogenic Belt show a trend toward more evolved negative eps Hf values with younging age from ca. 2.7–2.5 Ga without distinct peaks, which may suggest that an arc-continental collision initiated at ca. 2.5 Ga (Figure 12a). From these results, we interpret that the northern margin of the North China craton was affected by magmatism and collision-related deformation in both the Neoarchean Central Orogenic Belt and Paleoproterozoic Northern Margin orogen. The negative εHf(t) values correspond to ca. 1.9 and ca. 1.75 Ga on the εHf(t)-age plots for the Northern Margin orogen, which suggests the occurrence of continent-continent collision and crustal melting during that time (Figure 12b). In addition, the whole-rock Sr-Nd isotopic results from the Northern Margin orogen suggest that significant crustal growth and reworking occurred at ca. 2.70–2.55 Ga and ca. 2.5 Ga, respectively (e.g., Jian et al., 2012; X. Ma et al., 2016; X. Ma, Guo, et al., 2013; C. Wang et al., 2015; D. Wang et al., 2015; L. Wang et al., 2015; X. H. Zhang et al., 2014). Based on Sr-Nd-Pb-Hf isotopes, we interpret that the ca. 1.87–1.78 Ga post-collisional magmatism was sourced from partial melting of a subducted oceanic slab atop a continental magmatic arc, whereas the ca. 1.77–1.75 Ga Yanggao-Fengzhen mafic dykes and ca. 1.74–1.73 Ga Miyun mafic dykes were sourced from enriched mantle and prevalent/high-μ mantle magma sources, respectively (e.g., Han et al., 2020; Peng, 2015; Peng et al., 2022; Wu, Wang, et al., 2022; this study).

5.3. Paleoproterozoic Tectonic Evolution of the Northern North China Craton

Paleoproterozoic magmatism in the North China craton initiated at ca. 2.2 Ga in the Northern Margin orogen and Central Orogenic Belt. Previous studies suggested that a subduction-related continental arc was present from ca. 2.2–2.0 Ga, whereas several contemporaneous, extension-related A-type granitoids and mafic dykes have been reported in the central portion of the craton (Figure 14). Recent researchers suggest that prior to continent-continent collision, significant extension occurred in the upper plate during Andean-type subduction along the cratonal margin (e.g., Gün et al., 2021). Also, the major oxide, trace element, and isotope geochemical compositions of the A-type granitoids suggest that they were associated with differentiation of contemporaneous mafic rocks (J. Liu et al., 2021). Therefore, we propose that the ca. 2.2–2.0 Ga magmatic arc was related to the subduction event between the northern margin of the North China craton and another craton within the Columbia-Nuna

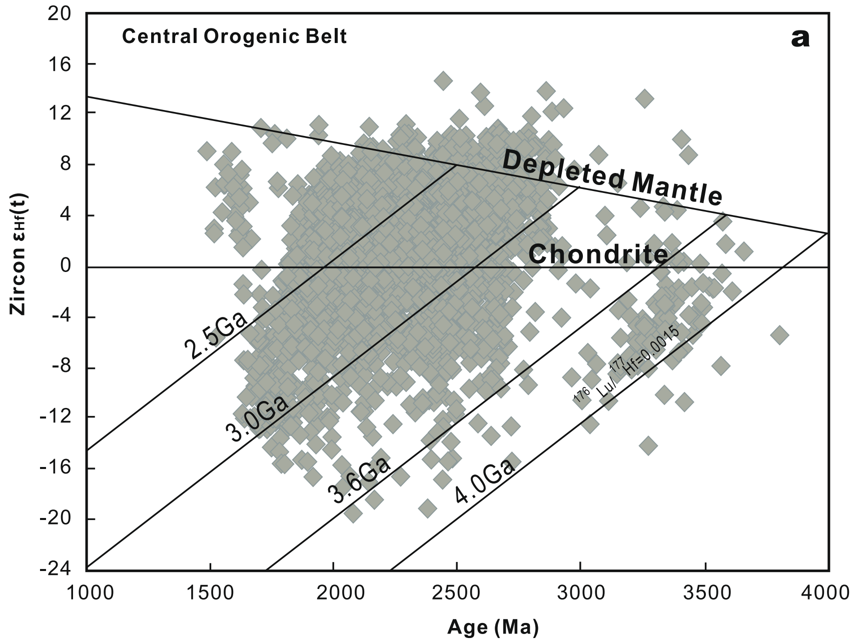

Figure 13. Plots of εHf(t) values versus U-Pb ages for the (a) Central Orogenic Belt and (b) Northern Margin orogen.

supercontinent along the Bayan Obo mélange (Wu et al., 2018) (Figures 14a and 14b). This interpretation is consistent with igneous zircon age populations with a ca. 1.95 Ga peak along the northern margin of the North China craton. Detrital zircon ages show that the maximum depositional age estimate of the Paleoproterozoic Hongqiyingzi Group quartzite is ca. 1.93 Ga. We observed the Hongqiyingzi Group quartzite to be folded due to ductile shear (Figure 14b). The ca. 1.93–1.80 Ga clockwise metamorphic *P–T* paths of high-pressure granulites of the northern North China craton margin are interpreted to be related to continent-continent collision and crustal thickening along the northern North China craton margin. In addition, ca. 1.87–1.80 Ga, post-collisional granitoids, mafic dykes, and carbonatites intrude Neoarchean ultramafic-mafic rocks and TTG gneiss (Figure 14c). The comparable ca. 1.90–1.85 Ga, post-collisional granitoids and dykes also occur along the southern margin of the North China craton, which reflects reworking by continent-continent collision of the northern and southern cratonal margins with outboard cratons of the Columbia-Nuna supercontinent during that time. This interpretation

10.1029/2022GC010662

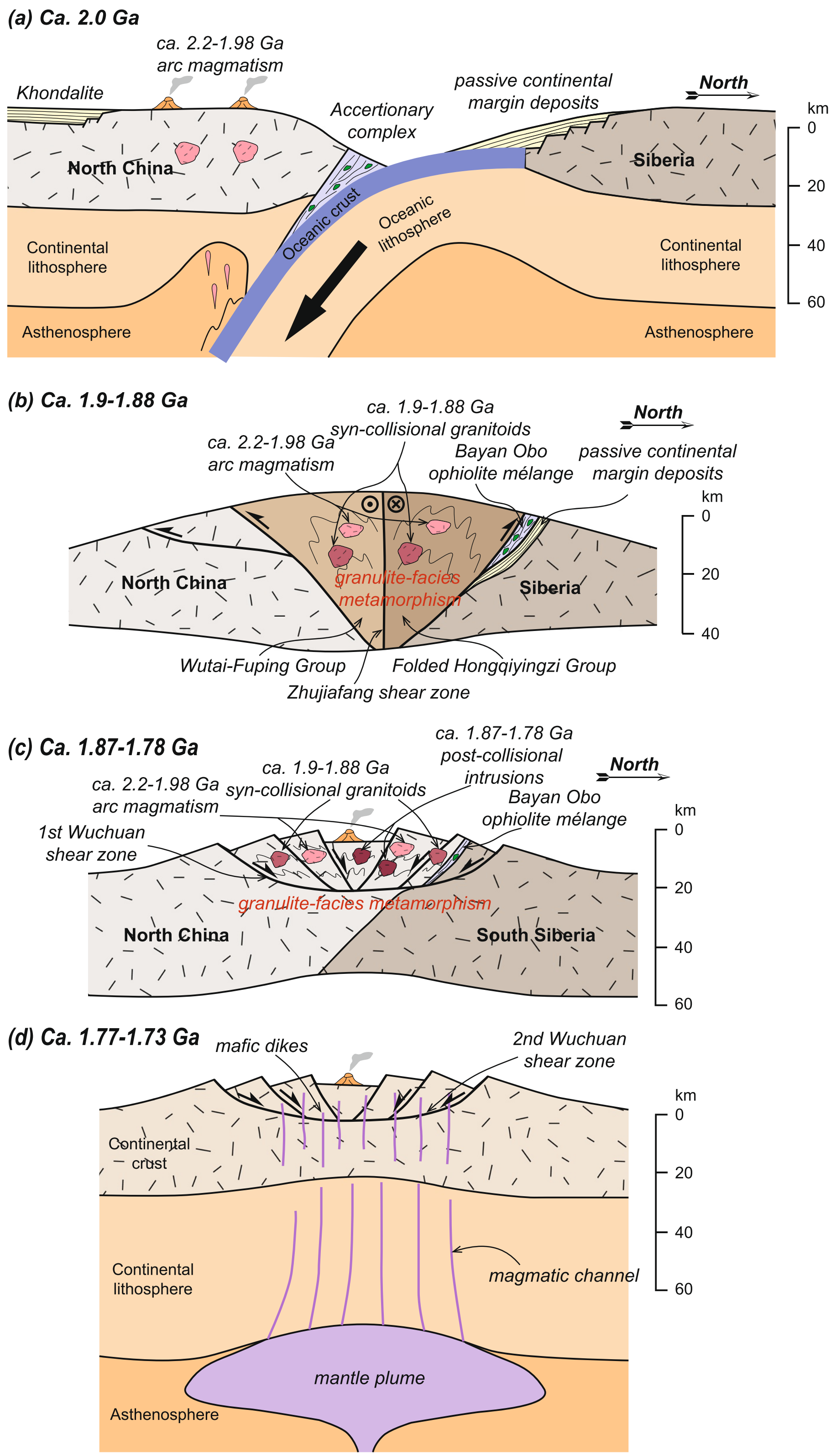

Figure 14. Tectonic evolution of the Northern Margin orogen in the North China craton.

is consistent with the metamorphic age population with a peak at ca. 1.85 Ga for the northern North China craton margin. Lastly, the ca. 1.78 Ga Yanggao plagioclase pyroxene granulite and ca. 1.77 Ga lamprophyre dykes are key evidence that continent-continent collision likely terminated by at least ca. 1.78 Ga (Figure 14c).

The Wuchuan mylonitic shear zones exposed along the northern margin of the North China craton contain at least two generations of ductile shearing. Wu, Wang, et al. (2022) interpreted that the earlier generation of shear foliation was associated with ca. 1.98–1.87 Ga Northern Margin orogenesis. Our new field observations and geochronology results indicate that the younger generation of shear foliation within the ca. 1.754 Ga granodiorite is crosscut by a ca. 1.73 Ga diorite dyke. Thus, we interpret that the youngest phase of Wuchuan ductile shear occurred between ca. 1.754 and 1.73 Ga. Several researchers suggest that a ca. 1.8–1.6 Ga mantle plume event occurred in the North China craton based on the occurrence of the ca. 1.78 Ga Xiong'er, ca. 1.77 Ga Taihang, ca. 1.73 Ga Miyun, ca. 1.68 Ga Laiwu, and ca. 1.63 Ga Taishan large igneous provinces. Peng et al. (2022) further proposed that the Xiong'er large igneous province represents the mantle plume center of the oldest hotspot track since ca. 1.8 Ga. They also interpret that the ca. 1.73 Ga Miyun large igneous province developed along the northern cratonal margin, which is consistent with the timing of the younger generation of ductile shear in Wuchuan (Figure 14d). The crust above the impinged mantle plume head may have experienced ductile or brittle-ductile deformation during broadscale extension (e.g., Birhanu et al., 2016; Gerya, 2014; Koptev et al., 2018) and/or along the flanks of thermally dirven buoyant upwellings in the crust (e.g., B. He et al., 2009; Roberts & Tikoff, 2021; J. Zuo et al., 2021; Zuza et al., 2022) (Figure 14d). The whole-rock concentrations of our ca. 1.77–1.76 Ga mafic dikes show lithospheric affinity, for example, depletion in Nb and Ta, but enriched in Th, U, and large ion lithophile elements such as Rb and La and enriched light rare earth elements. The negative εNd(t) varies from −7.4 to −21.3 and εHf(t) values range from −5.76 to −15.49; whereas their ^{206}Pb/^{204}Pbt and ^{207}Pb/^{204}Pbt vary between 16.8–17.5 and 15.4–15.5, respectively. In this scenario, crust affected by the mantle plume would experience voluminous dyke/sill intrusions, rapid uplift, heating and weakening of the mid-lower crust, the formation of progressively widening rifts (e.g., Buck, 1991; Campbell, 2005; Ernst & Buchan, 2003; Koptev et al., 2018; Morgan, 1971) coupled with possible crust scale buoyant upwellings driven by the partial melting of the lower crust. The occurrence of these processes in the North China craton is supported by the record of late Paleoproterozoic granulite- to amphibolite-facies metamorphism, widespread ca. 1.78–1.63 Ga mafic dyke/sills, and the Zha'ertai–Bayan Obo–Huade and Xiong'er rift zones along the northern and south margins of the craton (e.g., C. H. Liu et al., 2020; Peng, 2015; Peng et al., 2022; Zhai et al., 2000, 2015; S. H. Zhang et al., 2017; Zhou et al., 2018). In addition, detrital zircon ages for sedimentary rocks within the Zha'ertai–Bayan Obo–Huade rift along the northern cratonal margin show three major Neoarchean–Paleoproterozoic age populations of ca. 2.56–2.47 Ga, ca. 1.96–1.86 Ga, and ca. 1.78–1.62 Ga (e.g., C. H. Liu et al., 2020; Zhou et al., 2018), which are associated tectono-magmatic events that formed the Central Orogenic Belt, Northern Margin orogen, and large igneous provinces in the craton.

Ultimately, the Archean-Paleoproterozoic unique geologic history may have generated the thickened cratonic mantle keel to stabilize the North China craton. Cratonization may occur during repeated orogenesis (e.g., McKenzie & Priestley, 2016; Pearson et al., 2021) or mantle plume impingement (J. Liu et al., 2021; X. Xu et al., 2021). The two main phases of orogeny (e.g., 2.5 and 1.8 Ga) could have thickened the mantle lithosphere during progressive shortening. The subsequent ca. 1.8–1.6 Ga mantle plume event could have dehydrated and melt-depleted the continental mantle, and crustal heating and melting may have homogenized the composite North China crust. North China remained a relatively stable craton from the Paleoproterozoic until its destruction starting in the Mesozoic (e.g., Wu, Wang, et al., 2022).

The occurrence of ca. 2.2–2.0 Ga, subduction-related continental arcs are rare and thus, are useful for reconstructing the paleogeographic configuration of continents during the Paleoproterozoic (e.g., T. M. Kusky & Li, 2003; Wu et al., 2018, 2021; A. Yin et al., 2020; Zhao et al., 2002). The Northern Margin orogen of the North China craton consists mostly of Neoarchean supracrustal assemblages that are intruded by ca. 2.55–2.50 Ga felsic and ultramafic-mafic intrusions. These rocks were subsequently modified by ca. 1.98–1.87 Ga contraction evidenced by ductile folding, ca. 1.93–1.80 Ga granulite- to amphibolite-facies metamorphism, and ca. 2.2–2.0 Ga anatexis. These events were followed by ca. 1.90–1.88 Ga, north-south-oriented contraction and ca. 1.87–1.78 Ga post-collisional extension. The Northern Margin orogen is interpreted to be a possible Himalayan-style like collisional orogen (e.g., T. M. Kusky & Li, 2003; T. M. Kusky et al., 2016), similar to recent interpretations for the >600-km-long, Paleoproterozoic Limpopo orogenic belt of southern Africa (e.g., A. Yin et al., 2020) and other Paleoproterozoic orogens (Figure 15).

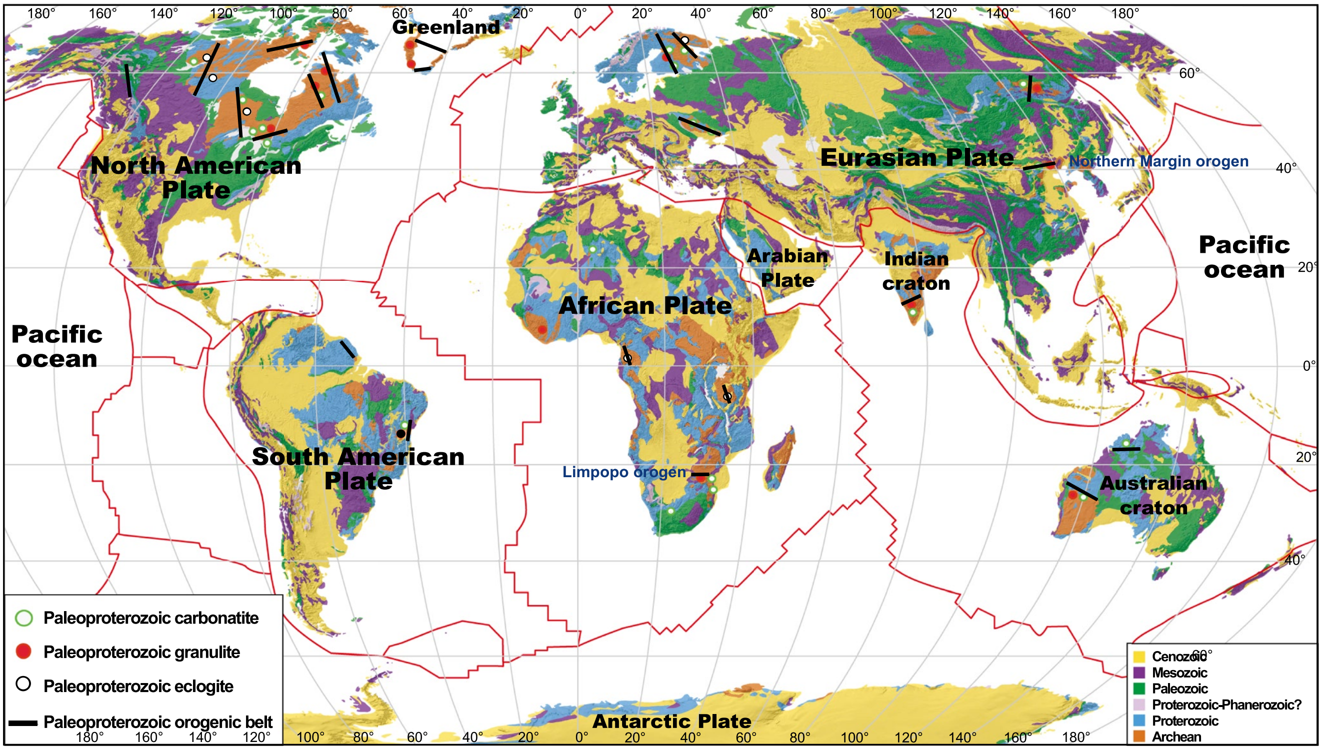

Figure 15. Global distribution of Paleoproterozoic (ca. 2.1–1.8 Ga) orogens that contain Paleoproterozoic carbonatites, granulites, and eclogites. Map is compiled from Zhao et al. (2002), C. Xu et al. (2018), and A. Yin et al. (2020). We propose that the east-trending Paleoproterozoic Northern Margin orogen developed as part of the North China craton.

The present-day Himalayan-Tibetan orogen and Tibetan Plateau contains records of preceding arc magmatism, ocean closure and major collisions, anatexis and leucogranite formation, granulite grade metamorphism, and a wide distributed zone of intra-plate deformation, Specifically, the eroded records of the modern Himalayan-Tibetan orogen would reveal phases of subduction-arc magmatism (e.g., initial subduction of the Meso-Tethys ocean) and subsequent collisional orogeny for longer than ∼200 Myr over an area with a north-south width >2,000 km (e.g., Kapp & DeCelles, 2019; Zuza et al., 2020). Therefore, tectonic reconstructions should consider that some of these major orogens, including the Northern Margin orogen, are not spatially restricted to narrow belts in time and space, but rather they likely persisted as broad, long-lived orogenic cycles that exist well within the intraplate continental interior. The hotter temperatures of Proterozoic orogens should have caused orogens to more laterally expansive but with more limited crustal thickening (Spencer et al., 2021). Here we have provided more support for the assertion that the Paleoproterozoic Northern Margin orogen stretched north-south over a distance of ∼200 km across the North China. In addition, we suggest that the western extent of Paleoproterozoic Northern Margin orogen may at least continue to the Longshou Shan of the western Alax block in the North China craton (Wu et al., 2021; Wu, Li et al., 2022), defining a west-east width of ∼1,600 km. These refined dimensions should be considered in attempts to restore the configuration of Archean-Paleoproterozoic cratons within supercontinents.

6. Conclusions

The Archean–Paleoproterozoic North China craton experienced two major arc magmatic and collisional events in the Neoarchean (ca. 2.5 Ga) and Paleoproterozoic (ca. 1.9 Ga), respectively, which are recorded in rocks exposed along the Northern Margin orogen. We present new field observations and results of zircon and baddeleyite U-Pb geochronology (11 samples), whole-rock major oxide and trace element geochemistry (12 samples), Sr-Nd-Pb-Hf isotope geochemistry (10 samples). In addition, we compiled detrital zircon ages and zircon Hf isotope data from across the Neoarchean Central Orogenic Belt and Paleoproterozoic Northern Margin orogen. Results including the occurrence of the ca. 1.84–1.78 Ga Yanggao granulite and 1.78 Ga lamprophyre intrusion led to interpretations, that a possible Himalayan-style continent-continent collision, with widespread intracontinental

Geochemistry, Geophysics, Geosystems 10.1029/2022GC010662

deformation, formed as a result of the Northern Margin orogen and terminated by 1.78 Ga. Ca. 1.77 Ga mafic dykes and ca. 1.75 Ga mylonitic shear zones exposed along the northern margin of the North China craton are possibly associated with a regional mantle plume event. Our results of arc magmatism, continental collision, and widely distributed intracontinental deformation are consistent that modern-style plate tectonics was operative by at least the late Paleoproterozoic.

Data Availability Statement

There are no restrictions on data usage. Zircon and baddeleyite analyses are archived at https://doi.org/10.26022/IEDA/112688, and our geochemical data are archived at https://doi.org/10.26022/IEDA/112689.

Acknowledgments

The authors thank Editor Whitney Behr, Associate Editor, and three anonymous reviewers for their constructive comments that have led to significant improvements of the original draft of this manuscript. This research was supported by Grants from the Basic Science Center for Tibetan Plateau Earth System (CTPES, Grant 41988101), the Second Tibetan Plateau Scientific Expedition and Research Program (Grant 2019QZKK0708), National Science Foundation of China (Grants 41772227 and 41702232), Tectonics Program of the National Science Foundation of U.S.A. (EAR 1914503 and EAR 1914501), and the Inner Mongolia Mapping Programs (Project Numbers 1212010811001, 1212011120700, DD20160045, and 1212010510506) administered by the Institute of Geological Survey, China University of Geosciences (Beijing). We thank Dr. Yahui Yue assistance in ICP-MS analyses. All data supporting the interpretations and conclusions of this study can be found in the manuscript text, the Supporting Information file, and specifically Tables S1 and S2 in Supporting Information S1.

References

Birhanu, Y., Bendick, R., Fisseha, S., Lewi, E., Floyd, M., King, R., & Reilinger, R. (2016). GPS constraints on broad scale extension in the Ethiopian Highlands and Main Ethiopian Rift. *Geophysical Research Letters*, *43*(13), 6844–6851. https://doi.org/10.1002/2016gl069890

Buck, W. R. (1991). Modes of continental extension. *Journal of Geophysics Research*, *96*(B2), 20161–20178. https://doi.org/10.1029/91jb01485

Cai, J., Liu, P., Ji, L., & Shi, J. (2017). Zircon geochronology of the Paleoproterozoic high-grade supracrustal rocks from the Huai'an Terrane, northwestern Hebei. *Acta Petrologica Sinica*, *33*(09), 2811–2826. [in Chinese with English abstract].

Campbell, I. H. (2005). Large igneous provinces and the mantle plume hypothesis. *Elements*, *1*(5), 265–269. https://doi.org/10.2113/gselements.1.5.265

Chen, X., Chen, Y., Li, D., Liu, Y., Wei, J., & Yan, J. (2015). LA-ICP-MS zircon U-Pb and Hf isotopic studies of the Wutai Group and their geological significance. *Geological Bulletin of Chin*, *34*(05), 861–876. [in Chinese with English abstract].

Cui, D., Chen, Y., Li, D., Wang, S., & Chen, X. (2015). Zircons U-Pb dating and Hf isotopic composition of clastic sedimentary rock in the Nansi Formation, Gantaohe Group, North China Craton and its tectonic significance. *Geological Review*, *61*(2), 425–442. [in Chinese with English abstract].

Dan, W., Li, X. H., Guo, J., Liu, Y., & Wang, X. C. (2012). Paleoproterozoic evolution of the eastern Alxa Block, westernmost North China: Evidence from in situ zircon U–Pb dating and Hf–O isotopes. *Gondwana Research*, *21*(4), 838–864. https://doi.org/10.1016/j.gr.2011.09.004

Dewey, J. F. (1969). Evolution of the Appalachian/Caledonian orogen. *Nature*, *222*(5189), 124–129. https://doi.org/10.1038/222124a0

Ding, J., Shi, Y., Kröner, A., & Lawford Anderson, J. (2018). Constraints on sedimentary ages of the Chuanlinggou Formation in the Ming Tombs, Beijing, North China Craton: LA-ICP-MS and SHRIMP U–Pb dating of detrital zircons. *Acta Geochimica*, *37*(2), 257–280. https://doi.org/10.1007/s11631-017-0211-1

Diwu, C., Sun, Y., Gao, J., & Fan, L. (2013). Early Precambrian tectonothermal events of the North China Craton: Constraints from in situ detrital zircon U-Pb, Hf and O isotopic compositions in Tietonggou Formation. *Chinese Science Bulletin*, *58*(31), 3760–3770. https://doi.org/10.1007/s11434-013-5817-z

Diwu, C., Sun, Y., Yuan, H., Wang, H., Zhong, X., & Liu, X. (2008). U-Pb ages and Hf isotopes for detrital zircons from quartzite in the Paleoproterozoic Songshan Group on the southwestern margin of the North China Craton. *Chinese Science Bulletin*, *53*(18), 2828–2839. https://doi.org/10.1007/s11434-008-0342-1

Diwu, C. R., Sun, Y., Lin, C. L., & Wang, H. L. (2010). LA-(MC)-ICPMS U-Pb zircon geochronology and Lu-Hf isotope compositions of the Taihua complex on the southern margin of the North China Craton. *Chinese Science Bulletin*, *55*(23), 2557–2571. https://doi.org/10.1007/s11434-010-3273-6

Dong, C., Liu, D., Li, J., Wang, Y., Zhou, H., Li, C., et al. (2007). Palaeoproterozoic Khondalite Belt in the western North China Craton: New evidence from SHRIMP dating and Hf isotope composition of zircons from metamorphic rocks in the Bayan Ul-Helan Mountains area. *Chinese Science Bulletin*, *52*(21), 2984–2994. https://doi.org/10.1007/s11434-007-0404-9

Dong, C., Wan, Y., Xu, Z., Liu, D., Yang, Z., Ma, M., & Xie, H. (2013). SHRIMP zircon U-Pb dating of late Paleoproterozoic kondalites in the Daqing Mountains area on the North China Craton. *Science China Earth Sciences*, *56*(1), 115–125. https://doi.org/10.1007/s11430-012-4459-3

Dong, X., Xu, Z., Liu, Z., & Sha, Q. (2012). Zircon U-Pb geochronology of Archean high-grade metamorphic rocks from Xi Ulanbulang area, central Inner Mongolia. *Science China Earth Sciences*, *55*(2), 204–212. https://doi.org/10.1007/s11430-011-4360-5

Du, L., Yang, C. Q., Wang, W., Ren, L., Wan, Y., Song, H., et al. (2011). The re-examination of the age and stratigraphic subdivision of the Hutuo Group in the Wutai Mountains area, North China Craton: Evidences from geology and zircon U-Pb geochronology. *Acta Petrologica Sinica*, *27*(04), 1037–1055. [in Chinese with English abstract].

Du, L., Yang, C. Q., Wang, W., Ren, L., Wan, Y., Song, H., et al. (2012). Provenance of the Paleoproterozoic Hutuo Group basal conglomerates and Neoarchean crustal growth in the Wutai Mountains, North China Craton: Evidence from granite and quartzite pebble zircon U-Pb ages and Hf isotopes. *Science China Earth Sciences*, *55*(11), 1796–1814. https://doi.org/10.1007/s11430-012-4407-2

Du, L., Yang, C. Q., Wyman, D. A., Nutman, A. P., Lu, Z., Song, H., et al. (2016). Age and depositional setting of the Paleoproterozoic Gantaohe Group in Zanhuang Complex: Constraints from zircon U–Pb ages and Hf isotopes of sandstones and dacite. *Precambrian Research*, *286*, 59–100. https://doi.org/10.1016/j.precamres.2016.09.027

Du, L., Yang, C. Q., Wyman, D. A., Nutman, A. P., Zhao, L., Lu, Z., et al. (2017). Zircon U-Pb ages and Lu-Hf isotope compositions from clastic rocks in the Hutuo Group: Further constraints on Paleoproterozoic tectonic evolution of the Trans-North China Orogen. *Precambrian Research*, *303*, 291–314. https://doi.org/10.1016/j.precamres.2017.04.007

Duan, C., Li, Y., Wei, M., Yang, Y., Hou, K., Chen, X., & Zhou, B. (2014). U-Pb dating study of detrital zircons from the Chuanlinggou Formation in Jiangjiazhai iron deposit, North China Craton and its geological significances. *Acta Petrologica Sinica*, *30*(01), 35–48. [in Chinese with English abstract].

Duan, C., Li, Y., Yang, Y., Liang, Y., Wei, M., & Hou, K. (2018). U-Pb ages and Hf isotopes of detrital zircon Grains from the Mesoproterozoic Chuanlinggou Formation in North China Craton: Implications for the Geochronology of sedimentary iron Deposits and Crustal evolution. *Minerals*, *8*(12), 547. https://doi.org/10.3390/min8120547

Ernst, R. E., & Buchan, K. L. (2003). Recognizing mantle plumes in the geological record. *Annual Review of Earth and Planetary Sciences*, *31*(1), 469–523. https://doi.org/10.1146/annurev.earth.31.100901.145500

Fan, H. R., Yan, K., Hu, F., Wang, K., & Zhai, M. G. (2010). Zircon geochronology of basement rocks from the Bayan Obo area, Inner Mongolia, and tectonic implications. *Acta Petrologica Sinica*, *26*(05), 1342–1350. [in Chinese with English abstract].
Faure, M., Trap, P., Lin, W., Monie, P., & Bruguier, O. (2007). Polyorogenic evolution of the paleoproterozoic Trans-North China Belt, new insights from the in Luliangshan-Hengshan-Wutaishan and Fuping massifs. *Episodes*, *30*(2), 95–106.
Gao, P., & Santosh, M. (2019). Building the Wutai arc: Insights into the Archean – Paleoproterozoic crustal evolution of the North China Craton. *Precambrian Research*, *333*, 105429. https://doi.org/10.1016/j.precamres.2019.105429
Geng, Y., Du, L., & Ren, L. (2012). Growth and reworking of the early Precambrian continental crust in the North China Craton: Constraints from zircon Hf isotopes. *Gondwana Research*, *21*(2), 517–529. https://doi.org/10.1016/j.gr.2011.07.006
Gerya, T. (2014). Precambrian geodynamics: Concepts and models. *Gondwana Research*, *25*(2), 442–463. https://doi.org/10.1016/j.gr.2012.11.008
Gün, E., Pysklywec, R. N., Göğüş, O. H., & Topuz, G. (2021). Pre-collisional extension of microcontinental terranes by a subduction pulley. *Nature Geoscience*, *14*(6), 443–450. https://doi.org/10.1038/s41561-021-00746-9
Guo, J., Zhai, M., & Xu, R. (2001). Timing of the granulite facies metamorphism in the Sanggan area, North China craton: Zircon U-Pb geochronology. *Science in China - Series D: Earth Sciences*, *44*(11), 1010–1018. https://doi.org/10.1007/bf02875394
Guo, J. H., Peng, P., Chen, Y., Jiao, S., & Windley, B. F. (2012). UHT sapphirine granulite metamorphism at 1.93–1.92 Ga caused by gabbronorite intrusions: Implications for tectonic evolution of the northern margin of the North China Craton. *Precambrian Research*, *222–223*, 124–142. https://doi.org/10.1016/j.precamres.2011.07.020
Guo, J. H., Zhai, M. G., Peng, P., Jiao, S., Zhao, L., & Wang, H. (2015). Paleoproterozoic granulites in the North China Craton and their geological implications. In *Precambrian Geology of China* (pp. 137–169). Springer.
Han, S. X., Wu, C., Zhou, Z. G., & Wang, G. S. (2020). Geology, geochemistry, and geochronology of the paleoproterozoic Donggouzi mafic-ultramafic complex: Implications for the evolution of the North China craton. *Lithos*, *366*, 105567. https://doi.org/10.1016/j.lithos.2020.105567
Harrison, T. M. (2020). *Hadean Earth* (p. 291). Springer Nature.
He, B., Xu, Y. G., & Paterson, S. (2009). Magmatic diapirism of the Fangshan pluton, southwest of Beijing, China. *Journal of Structural Geology*, *31*(6), 615–626. https://doi.org/10.1016/j.jsg.2009.04.007
He, X., Yin, C. Q., Long, X. P., Qian, J., Wang, L., & Qiao, H. (2017). Archean to Paleoproterozoic continental crust growth in the Western Block of North China: Constraints from zircon Hf isotopic and whole-rock Nd isotopic data. *Precambrian Research*, *303*, 105–116. https://doi.org/10.1016/j.precamres.2017.02.018
Heaman, L. M., & LeCheminant, A. N. (1993). Paragenesis and U-Pb systematics of baddeleyite (ZrO_2). *Chemical Geology*, *110*(1–3), 95–126. https://doi.org/10.1016/0009-2541(93)90249-i
Hu, G., Zhao, T., & Zhou, Y. (2014). Depositional age, provenance and tectonic setting of the Proterozoic Ruyang Group, southern margin of the North China Craton. *Precambrian Research*, *246*, 296–318. https://doi.org/10.1016/j.precamres.2014.03.013
Hu, G., Zhao, T., Zhou, Y., & Yan, Y. (2012). Depositional age and provenance of the Wufoshan Group in the southern margin of the North China Craton: Evidence from detrital zircon U-Pb ages and Hf isotopic compositions. *Geochimica*, *41*(04), 326–342. [in Chinese with English abstract].
Huang, B., Kusky, T., Johnson, T., Wilde, S., Wang, L., Polat, A., & Fu, D. (2020). Paired metamorphism in the Neoarchean: A record of accretionary-to-collisional orogenesis in the North China Craton. *Earth and Planetary Science Letters*, *543*, 116355. https://doi.org/10.1016/j.epsl.2020.116355
Jackson, S. E., Pearson, N. J., Griffin, W. L., & Belousova, E. A. (2004). The application of laser ablation-inductively coupled plasma-mass spectrometry to in situ U–Pb zircon geochronology. *Chemical Geology*, *211*(1–2), 47–69. https://doi.org/10.1016/j.chemgeo.2004.06.017
Jian, P., Kröner, A., Windley, B. F., Zhang, Q., Zhang, W., & Zhang, L. (2012). Episodic mantle melting-crustal reworking in the late Neoarchean of the northwestern North China Craton: Zircon ages of magmatic and metamorphic rocks from the Yinshan Block. *Precambrian Research*, *222–223*, 230–254. https://doi.org/10.1016/j.precamres.2012.03.002
Jian, P., Zhang, Q., Liu, D., Jin, W. X., Jia, X., & Qian, Q. (2005). SHRIMP dating and geological significance of Late Achaean high-Mg diorite (sanukite) and hornblende-granite at Guyang of Inner Monglia. *Acta Petrologica Sinica*, *21*(1), 153–159. [in Chinese with English abstract].
Jiao, S., Guo, J. H., Harley, S. L., & Windley, B. F. (2013). New Constraints from garnetite on the P–T path of the Khondalite Belt: Implications for the tectonic evolution of the North China Craton. *Journal of Petrology*, *54*(9), 1725–1758. https://doi.org/10.1093/petrology/egt029
Jin, W. (1989). *Early Precambrian geological evolution and metamorphic study on the basement of the north margin the North China platform*. (PhD thesis). Changchun College of Geology. (in Chinese).
Kapp, P., & DeCelles, P. G. (2019). Mesozoic–Cenozoic geological evolution of the Himalayan-Tibetan orogen and working tectonic hypotheses. *American Journal of Science*, *319*(3), 159–254. https://doi.org/10.2475/03.2019.01
Koptev, A., Calais, E., Burov, E., Leroy, S., & Gerya, T. (2018). Along-axis variations of rift width in a coupled lithosphere-mantle system, Application to East Africa. *Geophysical Research Letters*, *45*(11), 5362–5370. https://doi.org/10.1029/2018gl077276
Korenaga, J. (2018). Crustal evolution and mantle dynamics through Earth history. *Philosophical Transactions of the Royal Society A: Mathematical, Physical and Engineering Sciences*, *376*(2132), 20170408. https://doi.org/10.1098/rsta.2017.0408
Kröner, A., Wilde, S. A., Li, J. H., & Wang, K. Y. (2005). Age and evolution of a late Archean to Paleoproterozoic upper to lower crustal section in the Wutaishan/Hengshan/Fuping terrain of northern China. *Journal of Asian Earth Sciences*, *24*(5), 577–595. https://doi.org/10.1016/j.jseaes.2004.01.001
Kröner, A., Wilde, S. A., Zhao, G. C., O'Brien, J., Sun, M., Liu, D. Y., et al. (2006). Zircon geochronology and metamorphic evolution of mafic dykes in the Hengshan Complex of northern China: Evidence for late Palaeoproterozoic extension and subsequent high pressure metamorphism in the North China craton. *Precambrian Research*, *146*(1–2), 45–67. https://doi.org/10.1016/j.precamres.2006.01.008
Kusky, T., Huang, Y., Wang, L., Robinson, P. T., Wirth, R., Polat, A., & Wei, H. (2022). Vestiges of early Earth's deep subduction and CHONSP cycle recorded in Archean ophiolitic podiform chromitites. *Earth-Science Reviews*, *227*, 103968. https://doi.org/10.1016/j.earscirev.2022.103968
Kusky, T., Wang, J., Wang, L., Huang, B., Ning, W., Fu, D., & Shi, G. (2020). Mélanges through time: Life cycle of the world's largest Archean mélange compared with Mesozoic and Paleozoic subduction-accretion-collision mélanges. *Earth-Science Reviews*, *209*, 103303. https://doi.org/10.1016/j.earscirev.2020.103303
Kusky, T., Windley, B. F., Polat, A., Wang, L., Ning, W., & Zhong, Y. (2021). Archean dome-and-basin style structures form during growth and death of intraoceanic and continental margin arcs in accretionary orogens. *Earth-Science Reviews*, *220*, 103725. https://doi.org/10.1016/j.earscirev.2021.103725
Kusky, T. M., & Li, J. H. (2003). Paleoproterozoic tectonic evolution of the North China craton. *Journal of Asian Earth Sciences*, *22*(4), 383–397. https://doi.org/10.1016/S1367-9120(03)00071-3

Kusky, T. M., Li, J. H., & Santosh, M. (2007). The Paleoproterozoic North Hebei orogen: North China craton's collisional suture with the Columbia supercontinent. *Gondwana Research*, *12*(1–2), 4–28. https://doi.org/10.1016/j.gr.2006.11.012

Kusky, T. M., Polat, A., Windley, B. F., Burke, K. C., Dewey, J. F., Kidd, W. S. F., et al. (2016). Insights into the tectonic evolution of the North China craton through comparative tectonic analysis: A record of outward growth of Precambrian continents. *Earth-Science Reviews*, *162*, 387–432. https://doi.org/10.1016/j.earscirev.2016.09.002

Lan, C., Zhou, Y., Wang, C., & Zhao, T. (2017). Depositional age and protoliths of the Paleoproterozoic upper Taihua Group in the Wuyang area in the southern margin of the North China Craton: New insights into stratigraphic subdivision and tectonic setting. *Precambrian Research*, *297*, 77–100. https://doi.org/10.1016/j.precamres.2017.05.014

Lan, Z., Li, X., Chen, Z. Q., Li, Q., Hofmann, A., Zhang, Y., et al. (2014). Diagenetic xenotime age constraints on the Sanjiaotang Formation, Luoyu Group, southern margin of the North China Craton: Implications for regional stratigraphic correlation and early evolution of eukaryotes. *Precambrian Research*, *251*, 21–32. https://doi.org/10.1016/j.precamres.2014.06.012

Li, H., Lu, S., Su, W., Xiang, Z., Zhou, H., & Zhang, Y. (2013). Recent advances in the study of the Mesoproterozoic geochronology in the North China Craton. *Journal of Asian Earth Sciences*, *72*, 216–227. https://doi.org/10.1016/j.jseaes.2013.02.020

Li, M., Wang, C., & Wang, Z. (2013). Depositional age and geological implications of the Ruyang Group in the southwestern margin of the North China Craton: Evidence from detrital zircon U–Pb ages. *Chinese: The Journal of Geology*, *48*(4), 1115–1139. [in Chinese with English abstract].

Li, Q., Liu, S., Wang, Z., Chu, Z., Song, B., Wang, Y., & Wang, T. (2008). Contrasting provenance of Late Archean metasedimentary rocks from the Wutai Complex, North China Craton: Detrital zircon U–Pb, whole-rock Sm–Nd isotopic, and geochemical data. *International Journal of Earth Sciences*, *97*(3), 443–458. https://doi.org/10.1007/s00531-007-0170-6

Li, Q., Liu, S., Wang, Z., Shen, Y., Zhang, L., & Zhang, J. (2011). Provenance and geotectonic setting of the Palaeoproterozoic Zhongtiao Group and implications for assembly of the North China Craton: Whole-rock geochemistry and detrital zircon data. *Journal of the Geological Society*, *168*(5), 1215–1224. https://doi.org/10.1144/0016-76492010-146

Li, Q., Liu, S., Wang, Z., Zhang, F., Cheng, Y., & Wang, T. (2008). LA-ICP-MS U-Pb geochronology of the detrital zircons from the Jiangxian Group in the Zhongtiao Mountain and its tectonic significance. *Acta Petrologica Sinica*, *24*(06), 1359–1368. [in Chinese with English abstract].

Li, W. X., Yin, C., Lin, S., Li, W. J., Gao, P., Zhang, J., et al. (2022). Paleoproterozoic tectonic evolution from subduction to collision of the Khondalite Belt in North China: Evidence from multiple magmatism in the Qianlishan Complex. *Precambrian Research*, *368*, 106471. https://doi.org/10.1016/j.precamres.2021.106471

Li, X. P., Yang, Z., Zhao, G. C., Grapes, R., & Guo, J. H. (2011). Geochronology of khondalite-series rocks of the Jining Complex: Confirmation of depositional age and tectonometamorphic evolution of the North China craton. *International Geology Review*, *53*(10), 1194–1211. https://doi.org/10.1080/00206810903548984

Li, X. Y., Li, S., Wang, T. S., Dong, Y., Liu, X. G., Zhao, S. J., et al. (2020). Geochemistry and detrital zircon records of the Ruyang-Luoyu groups, southern North China Craton: Provenance, crustal evolution and Paleo–Mesoproterozoic tectonic implications. *Geoscience Frontiers*, *11*(2), 679–696. https://doi.org/10.1016/j.gsf.2019.08.003

Liu, C. H., Liu, F. L., Shi, J. R., Liu, P. H., Yang, H., Liu, L. S., et al. (2016). Depositional age and provenance of the Wutai Group: Evidence from zircon U–Pb and Lu–Hf isotopes and whole-rock geochemistry. *Precambrian Research*, *281*, 269–290. https://doi.org/10.1016/j.precamres.2016.06.002

Liu, C. H., Zhao, G. C., Liu, F. L., & Shi, J. (2014). Geochronological and geochemical constraints on the Lüliang Group in the Lüliang Complex: Implications for the tectonic evolution of the Trans-North China Orogen. *Lithos*, *198–199*, 298–315. https://doi.org/10.1016/j.lithos.2014.04.003

Liu, C. H., Zhao, G. C., Liu, F. L., Shi, J., & Ji, L. (2020). Detrital zircon records of late Paleoproterozoic to early Neoproterozoic northern North China Craton drainage reorganization: Implications for supercontinent cycles. *The Geological Society of America Bulletin*, *132*(9–10), 2135–2153. https://doi.org/10.1130/b35506.1

Liu, C. H., Zhao, G. C., Liu, F. L., Shi, J., Ji, L., Liu, P., et al. (2016). Zircon U–Pb and Lu–Hf isotopic and whole-rock geochemical constraints on the Lanhe and Heichashan Groups: Implications for the Paleoproterozoic tectonic basin evolution of the Lüliang Complex. *Lithos*, *262*, 526–545. https://doi.org/10.1016/j.lithos.2016.07.025

Liu, C. H., Zhao, G. C., Liu, F. L., Sun, M., Zhang, J., & Yin, C. Q. (2012). Zircons U-Pb and Lu-Hf isotopic and whole-rock geochemical constraints on the Gantaohe Group in the Zanhuang Complex: Implications for the tectonic evolution of the Trans-North China Orogen. *Lithos*, *146–147*, 80–92. https://doi.org/10.1016/j.lithos.2012.04.033

Liu, C. H., Zhao, G. C., Sun, M., Wu, F., Yang, J., Yin, C. Q., & Leung, W. H. (2011). U–Pb and Hf isotopic study of detrital zircons from the Yejishan Group of the Lüliang Complex: Constraints on the timing of collision between the eastern and Western Blocks, North China Craton. *Sedimentary Geology*, *236*(1), 129–140. https://doi.org/10.1016/j.sedgeo.2011.01.001

Liu, C. H., Zhao, G. C., Sun, M., Zhang, J., He, Y., Yin, C. Q., et al. (2011). U-Pb and Hf isotopic study of detrital zircons from the Hutuo group in the Trans-North China Orogen and tectonic implications. *Gondwana Research*, *20*(1), 106–121. https://doi.org/10.1016/j.gr.2010.11.016

Liu, C. H., Zhao, G. C., Sun, M., Zhang, J., & Yin, C. Q. (2012). U–Pb geochronology and Hf isotope geochemistry of detrital zircons from the Zhongtiao Complex: Constraints on the tectonic evolution of the Trans-North China Orogen. *Precambrian Research*, *222–223*, 159–172. https://doi.org/10.1016/j.precamres.2011.08.007

Liu, C. H., Zhao, G. C., Sun, M., Zhang, J., Yin, C. Q., & He, Y. (2012). Detrital zircon U–Pb dating, Hf isotopes and whole-rock geochemistry from the Songshan Group in the Dengfeng Complex: Constraints on the tectonic evolution of the Trans-North China Orogen. *Precambrian Research*, *192–195*, 1–15. https://doi.org/10.1016/j.precamres.2011.10.006

Liu, H., & Zhang, H. F. (2021). Chicheng high-pressure granulites record the paleoproterozoic tectonic evolution in the northern North China Craton. *Precambrian Research*, *359*, 106213. https://doi.org/10.1016/j.precamres.2021.106213

Liu, J., Pearson, D. G., Wang, L. H., Mather, K. A., Kjarsgaard, B. A., Schaeffer, A. J., et al. (2021). Plume-driven recratonization of deep continental lithospheric mantle. *Nature*, *592*(7856), 732–736. https://doi.org/10.1038/s41586-021-03395-5

Liu, J. H., Zhang, Q. W. L., Li, Z. M. G., Zhang, H. C. G., Chen, Y. C., & Wu, C. M. (2020). Metamorphic evolution and U-Pb geochronology of metapelite, northeastern Wutai Complex: Implications for paleoproterozoic tectonic evolution of the Trans-North China Orogen. *Precambrian Research*, *350*, 105928. https://doi.org/10.1016/j.precamres.2020.105928

Liu, L. C., Zhang, L. S., Dai, Y. P., Wang, C. L., & Li, Z. Q. (2012). Formation age, geochemical signatures and geological significance of the Sanheming BIF-type iron deposit in the Guyang greenstone belt, Inner Mongolia. *Acta Petrologica Sinica*, *28*(11), 3623–3637. [in Chinese with English abstract].

Liu, X., Zhang, J., Li, S., Li, X., & Yin, C. Q. (2020). Tectono-sedimentary evolution of the Mesoproterozoic basins in the southern Yan-Liao and Mianchi-Queshan areas: Insights from stratigraphic pattern and detrital zircon geochronology. *International Journal of Earth Sciences*, *109*(1), 43–62. https://doi.org/10.1007/s00531-019-01784-w

Lu, S. N., Yang, C. L., Li, H. K., & Li, H. M. (2002). A group of rifting events in the terminal Paleoproterozoic in the North China Craton. *Gondwana Research*, *5*(1), 123–131. https://doi.org/10.1016/s1342-937x(05)70896-0

Lu, S. N., Zhao, G. C., Wang, H. C., & Hao, G. J. (2008). Precambrian metamorphic basement and sedimentary cover of the North China Craton: A review. *Precambrian Research*, *160*(1–2), 77–93. https://doi.org/10.1016/j.precamres.2007.04.017

Ludwig, K. R. (2003). *ISOPLOT 3.0: A geochronological toolkit for Microsoft Excel* (pp. 1–70). Berkeley Geochronology Center Special Publication.

Lyu, Q. Q., Luo, S. S., Wang, T. S., Song, D. F., Tan, C., Zhang, Y., & Guan, Y. L. (2019). Detrital zircon U-Pb ages of the Zhaojiazhuang Formation, Middle–South section, Taihang Mountains, China and their geological significance. *Acta Geologica Sinica - English Edition*, *93*(3), 765–768. https://doi.org/10.1111/1755-6724.13785

Ma, M. Z., Wan, Y. S., Santosh, M., Xu, Z. Y., Xie, H. Q., Dong, C. Y., et al. (2012). Decoding multiple tectonothermal events in zircons from single rock samples: SHRIMP zircon U–Pb data from the late Neoarchean rocks of Daqingshan, North China Craton. *Gondwana Research*, *22*(3), 810–827. https://doi.org/10.1016/j.gr.2012.02.020

Ma, X., Fan, H. R., Santosh, M., & Guo, J. H. (2013). Geochemistry and zircon U–Pb chronology of charnockites in the Yinshan Block, North China Craton: Tectonic evolution involving Neoarchaean ridge subduction. *International Geology Review*, *55*(13), 1688–1704. https://doi.org/10.1080/00206814.2013.796076

Ma, X., Fan, H. R., Santosh, M., & Guo, J. H. (2016). Petrology and geochemistry of the Guyang hornblendite complex in the Yinshan block, North China Craton: Implications for the melting of subduction-modified mantle. *Precambrian Research*, *273*, 38–52. https://doi.org/10.1016/j.precamres.2015.12.001

Ma, X., Fan, H. R., Santosh, M., Liu, X., & Guo, J. H. (2014). Origin of sanukitoid and hornblendite enclaves in the Dajitu pluton from the Yinshan Block, North China Craton: Product of Neoarchaean ridge subduction? *International Geology Review*, *56*(10), 1197–1212. https://doi.org/10.1080/00206814.2014.929055

Ma, X., Guo, J. H., Liu, F., Qian, Q., & Fan, H. R. (2013). Zircon U–Pb ages, trace elements and Nd–Hf isotopic geochemistry of Guyang sanukitoids and related rocks: Implications for the Archean crustal evolution of the Yinshan Block, North China Craton. *Precambrian Research*, *230*, 61–78. https://doi.org/10.1016/j.precamres.2013.02.001

McDonough, W. F., & Sun, S. S. (1995). The composition of the Earth. *Chemical Geology*, *120*(3–4), 223–253. https://doi.org/10.1016/0009-2541(94)00140-4

McKenzie, D., & Priestley, K. (2016). Speculations on the formation of cratons and cratonic basins. *Earth and Planetary Science Letters*, *435*, 94–104. https://doi.org/10.1016/j.epsl.2015.12.010

Meert, J. G. (2012). What's in a name? The Columbia (Paleopangaea/Nuna) supercontinent. *Gondwana Research*, *21*(4), 987–993. https://doi.org/10.1016/j.gr.2011.12.002

Meng, J., Li, H., Li, L., & Li, J. (2018). Depositional time of the Tieshanmiao iron ore deposit in the Taihua Complex, Southern margin of the North China Craton: Constraint from zircon U-Pb dating and Hf isotope evidence. *Acta Geologica Sinica*, *92*(1), 125–141. [in Chinese with English abstract].

Meng, Y., Zuo, P. F., Zheng, D. S., Sun, F. B., Wang, P. X., Wang, Z. J., & Li, Y. (2018). The earliest clastic sediments overlying the Xiong'er volcanic rocks: Implications for the Mesoproterozoic tectonics of the southern North China Craton. *Precambrian Research*, *305*, 268–282. https://doi.org/10.1016/j.precamres.2017.12.001

Morgan, W. J. (1971). Convection plumes in the lover mantle. *Nature*, *30*(5288), 42–43. https://doi.org/10.1038/230042a0

Ning, W. B., Kusky, T. M., Wang, L., & Huang, B. (2022). Archean eclogite-facies oceanic crust indicates modern-style plate tectonics. *Proceedings of the National Academy of Sciences of the United States of America*, *119*(15), e2117529119. https://doi.org/10.1073/pnas.2117529119

Pearson, D. G., Scott, J. M., Liu, J., Schaeffer, A., Wang, L. H., van Hunen, J., et al. (2021). Deep continental roots and cratons. *Nature*, *596*(7871), 199–210. https://doi.org/10.1038/s41586-021-03600-5

Peng, P. (2015). Precambrian mafic dyke swarms in the North China Craton and their geological implications. *Science China Earth Sciences*, *58*(5), 649–675. https://doi.org/10.1007/s11430-014-5026-x

Peng, P., Feng, L., Sun, F., Yang, S., Su, X., Zhang, Z., & Wang, C. (2017). Dating the Gaofan and Hutuo Groups – Targets to investigate the paleoproterozoic great oxidation event in North China. *Journal of Asian Earth Sciences*, *138*, 535–547. https://doi.org/10.1016/j.jseaes.2017.03.001

Peng, P., Guo, J., Zhai, M., & Bleeker, W. (2010). Paleoproterozoic gabbronoritic and granitic magmatism in the northern margin of the North China Craton: Evidence of crust–mantle interaction. *Precambrian Research*, *183*(3), 635–659. https://doi.org/10.1016/j.precamres.2010.08.015

Peng, P., Wang, X. P., Windley, B. F., Guo, J. H., Zhai, M. G., & Li, Y. (2014). Spatial distribution of ~1950–1800 Ma metamorphic events in the North China craton: Implications for tectonic subdivision of the craton. *Lithos*, *202–203*, 250–266. https://doi.org/10.1016/j.lithos.2014.05.033

Peng, P., Xu, H., Mitchell, R. N., Teixeira, W., Kirscher, U., Qin, Z., et al. (2022). Earth's oldest hotspot track at ca. 1.8 Ga advected by a global subduction system. *Earth and Planetary Science Letters*, *585*, 117530. https://doi.org/10.1016/j.epsl.2022.117530

Peng, P., Zhai, M., Ernst, R. E., Guo, J., Liu, F., & Hu, B. (2008). A 1.78 Ga large igneous province in the North China craton: The Xiong'er Volcanic Province and the North China dyke swarm. *Lithos*, *101*(3–4), 260–280. https://doi.org/10.1016/j.lithos.2007.07.006

Peng, P., Zhai, M., Zhang, H., & Guo, J. (2005). Geochronological constraints on the paleoproterozoic evolution of the North China Craton: SHRIMP zircon ages of different types of mafic dikes. *International Geology Review*, *47*(5), 492–508. https://doi.org/10.2747/0020-6814.47.5.492

Qu, M., Guo, J., Lai, Y., Peng, P., & Liu, F. (2012). Origin and geological significance of the 1.81 Ga hyalophane-rich pegmatite veins from the high-pressure granulite terrain in the Central Zone of North China Craton. *Sci. China Earth Sci.*, *55*(2), 193–203. https://doi.org/10.1007/s11430-011-4330-y

Rämö, O. T., Haapala, I., Vaasjoki, M., Yu, J. H., & Fu, H. Q. (1995). 1700 Ma Shachang complex, northeast China: Proterozoic rapakivi granite not associated with Paleoproterozoic orogenic crust. *Geology*, *23*(9), 815–818. https://doi.org/10.1130/0091-7613(1995)023<0815:mscncp>2.3.co;2

Ren, L., Geng, Y., Du, L., Wang, Y., & Guo, J. H. (2013). SHRIMP data on zircons from the Wanzi series: Constraints on the rock formation time and implications of migmatization at 2.1–2.0 Ga in the Fuping Complex, North China Craton. *Journal of Asian Earth Sciences*, *72*, 203–215. https://doi.org/10.1016/j.jseaes.2012.12.041

Ren, R., Han, B., Zhang, Z., Li, J., Yang, Y., & Zhang, Y. (2011). Zircon U-Pb and Hf isotopic studies of basement gneiss and overlying Meso-Neoproterozoic sedimentary rocks from the Changping area, Beijing, and their geological implications. *Acta Petrologica Sinica*, *27*(06), 1721–1745. [in Chinese with English abstract].

Roberts, N. M., & Tikoff, B. (2021). Internal structure of the Paleoarchean Mt Edgar dome, Pilbara Craton, Western Australia. *Precambrian Research*, *358*, 106163. https://doi.org/10.1016/j.precamres.2021.106163

Rogers, J. J. W., & Santosh, M. (2002). Configuration of Columbia, a Mesoproterozoic supercontinent. *Gondwana Research*, *5*(1), 5–22. https://doi.org/10.1016/s1342-937x(05)70883-2

Santosh, M., Tsunogae, T., Li, J. H., & Liu, S. J. (2007). Discovery of sapphirine-bearing Mg-Al granulites in the North China Craton: Implications for Paleoproterozoic ultrahigh temperature metamorphism. *Gondwana Research*, *11*(3), 263–285. https://doi.org/10.1016/j.gr.2006.10.009

Santosh, M., Wilde, S. A., & Li, J. H. (2007). Timing of Paleoproterozoic ultrahigh temperature metamorphism in the North China Craton: Evidence from SHRIMP U-Pb zircon geochronology. *Precambr Res*, *159*(3–4), 178–196. https://doi.org/10.1016/j.precamres.2007.06.006

Santosh, M., Yang, Q.-Y., Teng, X., & Tang, L. (2015). Paleoproterozoic crustal growth in the North China Craton: Evidence from the Lüliang Complex. *Precambrian Research*, *263*, 197–231. https://doi.org/10.1016/j.precamres.2015.03.015

Shi, J., Yang, H., Yang, D., Wang, F., & Huo, T. (2018). Archean crustal growth and reconstruction of the southern margin of North China Craton: Constraints from the U-Pb-Hf isotopic compositions of detrital zircon from the Wuzhiling Formation at the Dengfeng area. *Geotectonica et Metallogenia*, *42*(02), 379–391. [in Chinese with English abstract].

Sláma, J., Košler, J., Condon, D. J., Crowley, J. L., Gerdes, A., Hanchar, J. M., et al. (2008). Plešovice zircon—A new natural reference material for U–Pb and Hf isotopic microanalysis. *Chemical Geology*, *249*(1–2), 1–35. https://doi.org/10.1016/j.chemgeo.2007.11.005

Spencer, C. J., Mitchell, R. N., & Brown, M. (2021). Enigmatic Mid-Proterozoic orogens: Hot, thin, and low. *Geophysical Research Letters*, *48*(16), e2021GL093312. https://doi.org/10.1029/2021gl093312

Stacey, J. T., & Kramers, J. D. (1975). Approximation of terrestrial lead isotope evolution by a two-stage model. *Earth and Planetary Science Letters*, *26*(2), 207–221. https://doi.org/10.1016/0012-821x(75)90088-6

Sun, Q., Zhou, Y., Zhao, T., Pang, L., & Qiu, Y. (2020). Geochronology and geochemistry of the Paleoproterozoic Fangniushan supracrustal strata in the Xiaoshan area, southern North China Craton: Implications for tectonic evolution. *Precambrian Research*, *346*, 105789. https://doi.org/10.1016/j.precamres.2020.105789

Sun, Q., Zhou, Y., Zhao, T., & Wang, W. (2017). Geochronology and geochemistry of the paleoproterozoic Yinyugou Group in the southern North China Craton: Implications for provenance and tectonic evolution. *Precambrian Research*, *296*, 120–147. https://doi.org/10.1016/j.precamres.2017.04.012

Tam, P. Y., Zhao, G., Liu, F., Zhou, X., Sun, M., & Li, S. (2011). Timing of metamorphism in the Paleoproterozoic Jiao-Liao-Ji Belt: New SHRIMP U-Pb zircon dating of granulites, gneisses and marbles of the Jiaobei massif in the North China craton. *Gondwana Research*, *19*(1), 150–162. https://doi.org/10.1016/j.gr.2010.05.007

Tang, L., Santosh, M., Tsunogae, T., & Maruoka, T. (2016). Paleoproterozoic meta-carbonates from the central segment of the Trans-North China Orogen: Zircon U–Pb geochronology, geochemistry, and carbon and oxygen isotopes. *Precambrian Research*, *284*, 14–29. https://doi.org/10.1016/j.precamres.2016.08.001

Trap, P., Faure, M., Lin, W., Le Breton, N., & Monie, P. (2012). Paleoproterozoic tectonic evolution of the Trans-North China orogen: Toward a comprehensive model. *Precambrian Research*, *222–223*, 191–211. https://doi.org/10.1016/j.precamres.2011.09.008

Trap, P., Faure, M., Lin, W., Monie, P., Meffre, S., & Melleton, J. (2009). The Zanhuang Massif, the second and eastern suture zone of the Paleoproterozoic Trans-North China orogen. *Precambrian Research*, *172*(1–2), 80–98. https://doi.org/10.1016/j.precamres.2009.03.011

Wan, B., Windley, B. F., Xiao, W., Feng, J., & Zhang, J. (2015). Paleoproterozoic high-pressure metamorphism in the northern North China craton and implications for the Nuna supercontinent. *Nature Communications*, *6*(1), 8344. https://doi.org/10.1038/ncomms9344

Wan, Y. S., Dong, C., Liu, D., Kröner, A., Yang, C., Wang, W., & Ma, M. (2012). Zircon ages and geochemistry of late Neoarchean syenogranites in the North China Craton: A review. *Precambrian Research*, *222*, 265–289. https://doi.org/10.1016/j.precamres.2011.05.001

Wan, Y. S., Liu, D., Dong, C., Xie, H., Kröner, A., Ma, M., et al. (2015). *Formation and evolution of Archean continental crust of the North China Craton*. *Precambrian Geology of China* (pp. 59–136). Springer.

Wan, Y. S., Liu, D., Dong, C., Xu, Z., Wang, Z., Wilde, S. A., et al. (2009). The Precambrian Khondalite Belt in the Daqingshan area, North China Craton: Evidence for multiple metamorphic events in the Palaeoproterozoic era. *Geological Society, London, Special Publications*, *323*(1), 73–97. https://doi.org/10.1144/sp323.4

Wan, Y. S., Liu, D., Wang, W., Song, T., Kröner, A., Dong, C., et al. (2011). Provenance of Meso- to Neoproterozoic cover sediments at the Ming Tombs, Beijing, North China Craton: An integrated study of U–Pb dating and Hf isotopic measurement of detrital zircons and whole-rock geochemistry. *Gondwana Research*, *20*(1), 219–242. https://doi.org/10.1016/j.gr.2011.02.009

Wan, Y. S., Miao, P., Liu, D., Yang, C., Wang, W., Wang, H., et al. (2010). Formation ages and source regions of the Palaeoproterozoic Gaofan, Hutuo and Dongjiao groups in the Wutai and Dongjiao areas of the North China Craton from SHRIMP U-Pb dating of detrital zircons: Resolution of debates over their stratigraphic relationships. *Chinese Science Bulletin*, *55*(13), 1278–1284. https://doi.org/10.1007/s11434-009-0615-3

Wan, Y. S., Song, B., Liu, D., Wilde, S. A., Wu, J., Shi, Y., et al. (2006). SHRIMP U–Pb zircon geochronology of Palaeoproterozoic metasedimentary rocks in the North China Craton: Evidence for a major Late Palaeoproterozoic tectonothermal event. *Precambrian Research*, *149*(3), 249–271. https://doi.org/10.1016/j.precamres.2006.06.006

Wang, C., Zhang, L., Dai, Y., & Lan, C. (2015). Geochronological and geochemical constraints on the origin of clastic meta-sedimentary rocks associated with the Yuanjiacun BIF from the Lüliang Complex, North China. *Lithos*, *212–215*, 231–246. https://doi.org/10.1016/j.lithos.2014.11.015

Wang, D., & Guo, J. (2017). Late Archean high-pressure pelitic granulites in the Yinshan Block, North China Craton. *Precambrian Research*, *303*, 251–267. https://doi.org/10.1016/j.precamres.2017.03.027

Wang, D., Guo, J. H., Huang, G., & Scheltens, M. (2015). The Neoarchean ultramafic–mafic complex in the Yinshan Block, North China Craton: Magmatic monitor of development of Archean lithospheric mantle. *Precambrian Research*, *270*, 80–99. https://doi.org/10.1016/j.precamres.2015.09.002

Wang, F., Chen, F., Siebel, W., Li, S. Q., Peng, P., & Zhai, M. G. (2011). Zircon U–Pb geochronology and Hf isotopic composition of the Hongqiyingzi Complex, northern Hebei Province: New evidence for paleoproterozoic and late Paleozoic evolution of the northern margin of the North China Craton. *Gondwana Research*, *20*(1), 122–136. https://doi.org/10.1016/j.gr.2011.02.003

Wang, J., Wu, Y., Gao, S., Peng, M., Liu, X., Zhao, L., et al. (2010). Zircon U–Pb and trace element data from rocks of the Huai'an Complex: New insights into the late paleoproterozoic collision between the Eastern and Western Blocks of the North China Craton. *Precambrian Research*, *178*(1), 59–71. https://doi.org/10.1016/j.precamres.2010.01.007

Wang, J. P., Kusky, T., Wang, L., Polat, A., Deng, H., Wang, C., & Wang, S. (2017). Structural relationships along a Neoarchean arc-continent collision zone, North China craton. *The Geological Society of America Bulletin*, *129*(1–2), 59–75. https://doi.org/10.1130/B31479.1

Wang, J. P., Li, X. W., Ning, W. B., Kusky, T., Wang, L., Polat, A., & Deng, H. (2019). Geology of a Neoarchean suture: Evidence from the Zunhua ophiolitic mélange of the Eastern Hebei Province, North China Craton. *The Geological Society of America Bulletin*, *131*(11–12), 1943–1964. https://doi.org/10.1130/B35138.1

Wang, L., Guo, J. H., Peng, P., Liu, F. L., & Windley, B. F. (2015). Lithological units at the boundary zone between the Jining and Huai'an Complexes (central-northern margin of the North China Craton): A paleoproterozoic tectonic mélange? *Lithos*, *227*, 205–224. https://doi.org/10.1016/j.lithos.2015.04.006

Wang, M., Zhou, H., & Zhang, H. (2020a). Detrital zircon geochronology and tectonic implications of the Mesoproterozoic Gaoshanhe Group in south margin of North China Craton. *Journal of Palaeogeography (Chinese Edition)*, *22*(01), 39–55. [in Chinese with English abstract].

Wang, M., Zhou, H., & Zhang, H. (2020b). Mesoproterozoic stratigraphic attribution and tectonic evolution in the southern margin of the North China Craton: Evidence from the detrital zircon U-Pb geochronology and zircon trace elements. *Acta Geologica Sinica*, *94*(04), 1027–1045. [in Chinese with English abstract].

Wang, X., Zhu, W. B., Liu, Y., Luo, M., Ge, R. F., Zhang, H., et al. (2017). Revisiting the Yejishan Group of the Lüliang Complex, North China: Implications for a paleoproterozoic active continental marginal basin in the Trans-North China Orogen. *Precambrian Research*, *292*, 93–114. https://doi.org/10.1016/j.precamres.2017.02.002

Wei, G. D., Kong, F. M., Liu, H., Wang, X. M., Zhang, Y. C., & Liu, X. H. (2019). Petrology, metamorphic PT paths and zircon U-Pb ages for Paleoproterozoic mafic granulites from Xuanhua, North China Craton. *Journal of Earth Science*, *30*(6), 1197–1214. https://doi.org/10.1007/s12583-019-1251-8

Wiedenbeck, M. A. P. C., Alle, P., Corfu, F. Y., Griffin, W. L., Meier, M., Oberli, F. V., et al. (1995). Three natural zircon standards for U-Th-Pb, Lu-Hf, trace element and REE analyses. *Geostandards Newsletter*, *19*(1), 1–23. https://doi.org/10.1111/j.1751-908x.1995.tb00147.x

Wu, C., Li, J., Zuza, A. V., Haproff, P. J., Yin, A., & Ding, L. (2022). Paleoproterozoic–paleozoic tectonic evolution of the Longshou Shan, western North China craton. *Geosphere*, *18*(3), 1177–1193. https://doi.org/10.1130/GES02491.1

Wu, C., Wang, G. S., Zhou, Z. G., Zhao, X. Q., & Haproff, P. J. (2022). Late Archean–Paleoproterozoic plate tectonics along the northern margin of the North China craton. *GSA Bulletin*. https://doi.org/10.1130/B36533.1

Wu, C., Zhou, Z. G., Zuza, A. V., Wang, G. S., Liu, C. F., & Jiang, T. (2018). A 1.9 Ga mélange along the northern margin of the North China craton: Implications for the assembly of Columbia supercontinent. *Tectonics*, *37*(10), 3610–3646. https://doi.org/10.1029/2018tc005103

Wu, C., Zuza, A. V., Yin, A., Chen, X. H., Haproff, P. J., Li, J., et al. (2021). Punctuated orogeny during the assembly of Asia: Tectonostratigraphic evolution of the North China Craton and the Qilian Shan from the paleoproterozoic to early Paleozoic. *Tectonics*, *40*(4), e2020TC006503. https://doi.org/10.1029/2020tc006503

Xia, X. P., Sun, M., Zhao, G. C., & Luo, Y. (2006). LA-ICP-MS U–Pb geochronology of detrital zircons from the Jining Complex, North China Craton and its tectonic significance. *Precambrian Research*, *144*(3), 199–212. https://doi.org/10.1016/j.precamres.2005.11.004

Xia, X. P., Sun, M., Zhao, G. C., Wu, F. Y., & Xie, L. (2009). U–Pb and Hf isotopic study of detrital zircons from the Lüliang khondalite, North China Craton, and their tectonic implications. *Geological Magazine*, *146*(5), 701–716. https://doi.org/10.1017/s0016756809006396

Xia, X. P., Sun, M., Zhao, G. C., Wu, F. Y., Xu, P., Zhang, J., & He, Y. H. (2008). Paleoproterozoic crustal growth in the Western Block of the North China Craton: Evidence from detrital zircon Hf and whole rock Sr-nd isotopic compositions of the Khondalites from the Jining Complex. *American Journal of Science*, *308*(3), 304–327. https://doi.org/10.2475/03.2008.05

Xiao, D., Ning, W. B., Wang, J. P., Kusky, T., Wang, L., Deng, H., et al. (2021). Neoarchean to Paleoproterozoic tectonothermal evolution of the North China Craton: Constraints from geological mapping and Th-U-Pb geochronology of zircon, titanite, and monazite in Zanhuang massif. *Precambrian Research*, *359*, 106214. https://doi.org/10.1016/j.precamres.2021.106214

Xiao, L. L., Clarke, G., Liu, F. L., & Lu, J. S. (2019). Metamorphic records in the Lüliang metapelites of the Jiehekou Group: Implications for the tectonic evolution of the Trans-North China Orogen, North China Craton. *Precambrian Research*, *332*, 105415. https://doi.org/10.1016/j.precamres.2019.105415

Xie, L., Zhang, Y., Zhang, H., Sun, J., & Wu, F. (2008). In situ simultaneous determination of trace elements, U-Pb and Lu-Hf isotopes in zircon and baddeleyite. *Chinese Science Bulletin*, *53*(10), 1565–1573. https://doi.org/10.1007/s11434-008-0086-y

Xu, C., Kynicky, J., Song, W. L., Tao, R. B., Lü, Z., Li, Y. X., et al. (2018). Cold deep subduction recorded by remnants of a Paleoproterozoic carbonated slab. *Nature Communications*, *9*(1), 2790. https://doi.org/10.1038/s41467-018-05140-5

Xu, X., Zuza, A. V., Yin, A., Lin, X., Chen, H., & Yang, S. (2021). Permian plume-strengthened Tarim lithosphere controls the Cenozoic deformation pattern of the Himalayan-Tibetan orogen. *Geology*, *49*(1), 96–100. https://doi.org/10.1130/g47961.1

Yang, Q. Y., Santosh, M., & Tsunogae, T. (2014). Ultrahigh-temperature metamorphism under isobaric heating: New evidence from the North China Craton. *Journal of Asian Earth Sciences*, *95*, 2–16. https://doi.org/10.1016/j.jseaes.2014.01.018

Yin, A. (2012). An episodic slab-rollback model for the origin of the Tharsis rise on Mars: Implications for initiation of local plate subduction and final unification of a kinematically linked global plate-tectonic network on Earth. *Lithosphere*, *4*(6), 553–593. https://doi.org/10.1130/l195.1

Yin, A., Brandl, G., & Kröner, A. (2020). Plate-tectonic processes at ca. 2.0 Ga: Evidence from >600 km of plate convergence. *Geology*, *48*(2), 103–107. https://doi.org/10.1130/g47070.1

Yin, C. Q., Zhao, G. C., Guo, J. H., Sun, M., Xia, X. P., Zhou, X., & Liu, C. H. (2011). U–Pb and Hf isotopic study of zircons of the Helanshan Complex: Constrains on the evolution of the Khondalite Belt in the Western Block of the North China Craton. *Lithos*, *122*(1), 25–38. https://doi.org/10.1016/j.lithos.2010.11.010

Yin, C. Q., Zhao, G. C., Sun, M., Xia, X. P., Wei, C., Zhou, X., & Leung, W. (2009). LA-ICP-MS U–Pb zircon ages of the Qianlishan Complex: Constrains on the evolution of the Khondalite Belt in the Western Block of the North China Craton. *Precambrian Research*, *174*(1), 78–94. https://doi.org/10.1016/j.precamres.2009.06.008

Zhai, M. G. (2011). Cratonization and the ancient North China continent: A summary and review. *Science China Earth Sciences*, *54*(8), 1110–1120. https://doi.org/10.1007/s11430-011-4250-x

Zhai, M. G. (2014). Multi-stage crustal growth and cratonization of the North China craton. *Geoscience Frontiers*, *5*(4), 457–469. https://doi.org/10.1016/j.gsf.2014.01.003

Zhai, M. G., Bian, A., & Zhao, T. (2000). The amalgamation of the supercontinent of North China Craton at the end of Neo-Archaean and its breakup during late Palaeoproterozoic and Meso-Proterozoic. *Science in China Series D: Earth Sciences*, *43*(1), 219–232. https://doi.org/10.1007/BF02911947

Zhai, M. G., Guo, J. H., Yan, Y. H., Li, Y. G., & Han, X. L. (1992). Discovery of high pressure basic granulite terrain in North China craton and preliminary study. *Science in China - Series E: Technological Sciences*, *12*, 1325–1330.

Zhai, M. G., Guo, J. H., Yan, Y. H., Li, Y. G., & Han, X. L. (1993). Discovery of high pressure basic granulite terrain in North China Archean craton and preliminary study. *Science in China - Series E: Technological Sciences*, *36*, 1402–1408.

Zhai, M. G., Hu, B., Zhao, T., Peng, P., & Meng, Q. (2015). Late Paleoproterozoic–Neoproterozoic multi-rifting events in the North China Craton and their geological significance: A study advance and review. *Tectonophysics*, *662*, 153–166. https://doi.org/10.1016/j.tecto.2015.01.019

Zhai, M. G., & Santosh, M. (2011). The early Precambrian odyssey of the North China craton: A synoptic overview. *Gondwana Research*, *20*(1), 6–25. https://doi.org/10.1016/j.gr.2011.02.005

Zhai, M. G., Zhao, L., Zhu, X. Y., Zhou, Y. Y., Peng, P., Guo, J. H., et al. (2021). Late Neoarchean magmatic–metamorphic event and crustal stabilization in the North China Craton. *American Journal of Science*, *321*(1–2), 206–234. https://doi.org/10.2475/01.2021.06

Zhang, D. D., O'Brien, P. J., Schertl, H. P., Ma, X., Tian, Z., Zhao, L., & Guo, J. (2021). Metamorphic and geochronological evolution of Paleoproterozoic high-pressure ultra-high-temperature pelitic granulite, Chicheng, northern Trans-North China Orogen. *Precambrian Research*, *361*, 106237. https://doi.org/10.1016/j.precamres.2021.106237

Zhang, F., Wang, Y. B., Du, L. L., Yang, C. H., Ayers, J. C., & Yuan, H. Q. (2019). The Neoarchean-paleoproterozoic volcanic-sedimentary rocks in the Zanhuang Complex, North China Craton: Petrogenesis and implications for tectonic evolution. *Precambrian Research*, *328*, 64–80. https://doi.org/10.1016/j.precamres.2019.03.015

Zhang, H. C., Zhao, G., Wang, C., Yao, J., & Xu, N. (2022). Phase equilibria modelling and zircon U-Pb geochronology of Paleoproterozoic mafic granulites from the Chengde Complex, North China Craton. *Precambrian Research*, *371*, 106576. https://doi.org/10.1016/j.precamres.2022.106576

Zhang, H. F., Wang, J. L., Zhou, D. W., Yang, Y. H., Zhang, G. W., Santosh, M., et al. (2014). Hadean to Neoarchean episodic crustal growth: Detrital zircon records in Paleoproterozoic quartzites from the southern North China Craton. *Precambrian Research*, *254*, 245–257. https://doi.org/10.1016/j.precamres.2014.09.003

Zhang, H. F., Zhang, J., Zhang, G. W., Santosh, M., Yu, H., Yang, Y. H., & Wang, J. L. (2016). Detrital zircon U–Pb, Lu–Hf, and O isotopes of the Wufoshan Group: Implications for episodic crustal growth and reworking of the southern North China craton. *Precambrian Research*, *273*, 112–128. https://doi.org/10.1016/j.precamres.2015.12.004

Zhang, S. H., Liu, S. W., Zhao, Y., Yang, J. H., Song, B., & Liu, X. M. (2007). The 1.75–1.68 Ga anorthosite-mangerite-alkali granitoid-rapakivi granite suite from the northern North China Craton: Magmatism related to a Paleoproterozoic orogen. *Precambrian Research*, *155*(3–4), 287–312. https://doi.org/10.1016/j.precamres.2007.02.008

Zhang, S. H., Zhao, Y., Li, X. H., Ernst, R. E., & Yang, Z. Y. (2017). The 1.33–1.30 Ga Yanliao large igneous province in the North China Craton: Implications for reconstruction of the Nuna (Columbia) supercontinent, and specifically with the North Australian Craton. *Earth and Planetary Science Letters*, *465*, 112–125. https://doi.org/10.1016/j.epsl.2017.02.034

Zhang, S. H., Zhao, Y., Yang, Z. Y., He, Z. F., & Wu, H. (2009). The 1.35 Ga diabase sills from the northern North China Craton: Implications for breakup of the Columbia (Nuna) supercontinent. *Earth and Planetary Science Letters*, *288*(3–4), 588–600. https://doi.org/10.1016/j.epsl.2009.10.023

Zhang, W., & Hu, Z. C. (2020). Estimation of isotopic reference values for pure materials and geological reference materials. *Atomic Spectroscopy*, *41*(3), 93–102. https://doi.org/10.46770/as.2020.03.001

Zhang, W., Hu, Z. C., & Liu, Y. S. (2020). Iso-Compass: New freeware software for isotopic data reduction of LA-MC-ICP-MS. *Journal of Analytical Atomic Spectrometry*, *35*(6), 1087–1096. https://doi.org/10.1039/d0ja00084a

Zhang, X. H., Yuan, L. L., Xue, F. H., & Zhai, M. G. (2014). Neoarchean metagabbro and charnockite in the Yinshan block, western North China Craton: Petrogenesis and tectonic implications. *Precambrian Research*, *255*, 563–582. https://doi.org/10.1016/j.precamres.2013.11.003

Zhao, G., & Cawood, P. A. (2012). Precambrian geology of China. *Precambrian Research*, *222–223*, 13–54. https://doi.org/10.1016/j.precamres.2012.09.017

Zhao, G., Cawood, P. A., Li, S., Wilde, S. A., Sun, M., Zhang, J., & Yin, C. (2012). Amalgamation of the North China Craton: Key issues and discussion. *Precambrian Research*, *222*, 55–76. https://doi.org/10.1016/j.precamres.2012.09.016

Zhao, G., Cawood, P. A., Wilde, S. A., & Sun, M. (2002). Review of the global 2.1–1.8 Ga orogens: Implications for a pre-Rodinian supercontinent. *Earth-Science Reviews*, *59*(1–4), 125–162. https://doi.org/10.1016/s0012-8252(02)00073-9

Zhao, G., Sun, M., Wilde, S. A., & Li, S. (2004). A Paleo-Mesoproterozoic supercontinent: Assembly, growth and breakup. *Earth-Science Reviews*, *67*(1–2), 91–123. https://doi.org/10.1016/j.earscirev.2004.02.003

Zhao, G., Sun, M., Wilde, S. A., & Li, S. Z. (2005). Late Archean to Paleoproterozoic evolution of the North China Craton: Key issues revisited. *Precambrian Research*, *136*(2), 77–202. https://doi.org/10.1016/j.precamres.2004.10.002

Zhao, G., Wilde, S. A., Cawood, P. A., & Sun, M. (2001). Archean blocks and their boundaries in the North China craton: Lithological, geochemical, structural and P-T path constraints and tectonic evolution. *Precambrian Research*, *107*(1–2), 45–73. https://doi.org/10.1016/s0301-9268(00)00154-6

Zhao, G., Wilde, S. A., Sun, M., Guo, J. H., Kroner, A., Li, S. Z., et al. (2008). SHRIMP U-Pb zircon geochronology of the Huai'an Complex: Constraints on Late Archean to paleoproterozoic magmatic and metamorphic events in the Trans-North China Orogen. *American Journal of Science*, *308*(3), 270–303. https://doi.org/10.2475/03.2008.04

Zhao, G., & Zhai, M. G. (2013). Lithotectonic elements of Precambrian basement in the North China Craton: Review and tectonic implications. *Gondwana Research*, *23*(4), 1207–1240. https://doi.org/10.1016/j.gr.2012.08.016

Zhong, Y., Kusky, T. M., & Wang, L. (2022). Giant sheath-folded nappe stack demonstrates extreme subhorizontal shear strain in an Archean orogen. *Geology*, *50*(5), 577–582. https://doi.org/10.1130/G49599.1

Zhong, Y. T., Kusky, T., Wang, L., Polat, A., Liu, X. Y., Peng, Y. Y., et al. (2021). Alpine-style nappes thrust over ancient North China continental margin demonstrate large Archean horizontal plate motions. *Nature Communications*, *12*(1), 6172. https://doi.org/10.1038/s41467-021-26474-7

Zhou, Z. G., Hu, M. M., Wu, C., Wang, G. S., Liu, C. F., Cai, A. R., & Jiang, T. (2018). Coupled U–Pb dating and Hf isotopic analysis of detrital zircons from Bayan Obo Group in Inner Mongolia: Constraints on the evolution of the Bayan Obo rift belt. *Geological Journal*, *53*(6), 2649–2664. https://doi.org/10.1002/gj.3102

Zhu, X. Y., Chen, F., Li, S. Q., Yang, Y. Z., Nie, H., Siebel, W., & Zhai, M. G. (2011). Crustal evolution of the North Qinling terrain of the Qinling Orogen, China: Evidence from detrital zircon U–Pb ages and Hf isotopic composition. *Gondwana Research*, *20*(1), 194–204. https://doi.org/10.1016/j.gr.2010.12.009

Zhu, X. Y., Qiu, Y., Pang, L., & Zhai, M. G. (2019). Multi-source of clastic sedimentary rocks in the Gaoshanhe Group along the southern margin of the North China Craton: Implications for regional stratum comparison and tectonic evolution. *Acta Petrologica Sinica*, *35*(8), 2487–2502. (in Chinese with English abstract).

Zuo, J., Webb, A. A. G., Piazolo, S., Wang, Q., Müller, T., Ramírez-Salazar, A., & Haproff, P. J. (2021). Tectonics of the Isua supracrustal belt 2: Microstructures reveal distributed strain in the absence of major fault structures. *Tectonics*, *40*(3), e2020TC006514. https://doi.org/10.1029/2020tc006514

Zuo, P., Li, Y., Liu, S., & Zheng, D. (2019). Meso-Neoproterozoic sedimentary evolution of the southern margin of the North China Craton: Evidence from the Huanglianduo and Dongjia formations in the western Henan. *Acta Petrologica Sinica*, *35*(08), 2545–2572. [in Chinese with English abstract]. https://doi.org/10.18654/1000-0569/2019.08.14

Zuo, P., Li, Y., Zhang, G., Si, R., Wang, S., Liu, S., et al. (2019). Reviews of the Mesoproterozoic to Neoproterozoic sedimentary sequences and new constraints on the tectono-sedimentary evolution of the southern margin of the North China Craton. *Journal of Asian Earth Sciences*, *179*, 416–429. https://doi.org/10.1016/j.jseaes.2019.04.010

Zuo, X., Qiu, Y., Pang, L., & Zhai, M. G. (2019). Multi-source of elastic sedimentary rocks in the Gaoshanhe Group along the southern margin of the North China Craton: Implications for regional stratum comparison and tectonic evolution. *Acta Petrologica Sinica*, *35*(08), 2487–2502. [in Chinese with English abstract]. https://doi.org/10.18654/1000-0569/2019.08.11

Zuza, A. V., Gavillot, Y., Haproff, P. J., & Wu, C. (2020). Kinematic evolution of a continental collision: Constraining the Himalayan-Tibetan orogen via bulk strain rates. *Tectonophysics*, *797*, 228642. https://doi.org/10.1016/j.tecto.2020.228642

Zuza, A. V., Levy, D. A., Dee, S., DesOrmeau, J. W., Cheng, F., & Li, X. (2022). Structural architecture and attenuation of the ductile lower plate of the Ruby Mountain-East Humboldt Range metamorphic core complex, Northeast Nevada. *Tectonics*, *41*(8), e2021TC007162. https://doi.org/10.1029/2021tc007162

Zuza, A. V., & Yin, A. (2017). Balkatach hypothesis: A new model for the evolution of the Pacific, Tethyan, and Paleo-Asian oceanic domains. *Geosphere*, *13*(5), 1664–1712. https://doi.org/10.1130/ges01463.1